Prepared for publication as a <u>Tutorial Review</u> in <i>Analytica Chimica Acta</i>
Tutorial Review: Enrichment and Separation of Neutral and Charged Species by Ion Concentration Polarization Focusing
Beatrise Berzina, ^a Robbyn K. Anand ^a *
^a The Department of Chemistry, Iowa State University, 2415 Osborn Drive, 1605 Gilman Hall,
Ames, Iowa 50011-1021, United States.
Keywords: Ion concentration polarization, focusing, enrichment, separation, electrokinetics
*To whom the correspondence should be addressed
*E-mail: rkanand@iastate.edu
Submitted: April 3, 2020

ABSTRACT

Ion concentration polarization focusing (ICPF) is an electrokinetic technique, in which analytes are enriched and separated along a localized electric field gradient in the presence of a counter flow. This field gradient is generated by depletion of ions of the background electrolyte at an ion permselective junction. In this tutorial review, we summarize the fundamental principles and experimental parameters that govern selective ion transport and the stability of the enriched analyte plug. We also examine faradaic ICP (fICP), in which local ion concentration is modulated via electrochemical reactions as an attractive alternative to ICP that achieves similar performance with a decrease in both power consumption and Joule heating. The tutorial covers important challenges to the broad application of ICPF including undesired pH gradients, low volumetric throughput, samples that induce biofouling or are highly conductive, and limited approaches to on- or off- chip analysis. Recent developments in the field that seek to address these challenges are reviewed along with new approaches to maximize enrichment, focus uncharged analytes, and achieve enrichment and separation in water-in-oil droplets. For new practitioners, we discuss practical aspects of ICPF, such as strategies for device design and fabrication and the relative advantages of several types of ion selective junctions and electrodes. Lastly, we summarize tips and tricks for tackling common experimental challenges in ICPF.

Table of Contents

- 1. Introduction
- 2. Fundamental aspects of ion concentration polarization (ICP)
 - 2.1. Mechanism of ICP
 - 2.2. Mechanism of faradaic ICP (fICP)
 - 2.3. Electric and flow fields that drive ICP focusing (ICPF)
 - 2.4. Secondary electroosmotic flow (EOF) or vortex flow
 - 2.5. Propagation of the ion depletion zone (IDZ) boundary
 - 2.6. Spatiotemporal pH dynamics near ion selective membranes and electrodes during ICP
- 3. Practical aspects of implementing ICP-based techniques
 - 3.1. Device design and fabrication methods
 - 3.2. Ion selective features and their fabrication
 - 3.2.1. Ion permselective membranes and hydrogels
 - 3.2.2. Bead beds
 - 3.2.3. Nanotubes
 - 3.2.4. Electrodes for fICP
 - 3.3. Sample composition
 - 3.3.1. Concentration of the analyte and the electrolyte determine the limit of enrichment
 - 3.3.2. Complex matrices in biological applications
 - 3.3.3. Additives to the sample for sharper IDZ boundary formation
 - 3.3.4. Additives to alter analyte mobility and to achieve focusing of uncharged species
 - 3.4. Analyte encapsulation following ICP
 - 3.5. In-droplet ICP

- 3.6. Multistage and high-throughput preconcentration
- 4. Integration of other analytical methods with ICPF
 - 4.1. Immunoassay
 - 4.2. Enzymatic assay
 - 4.3. Electrochemical sensing
 - 4.4. The ICP current-voltage curve as a non-optical sensor
- 5. Summary of tips and tricks
- 6. Conclusions and future outlook

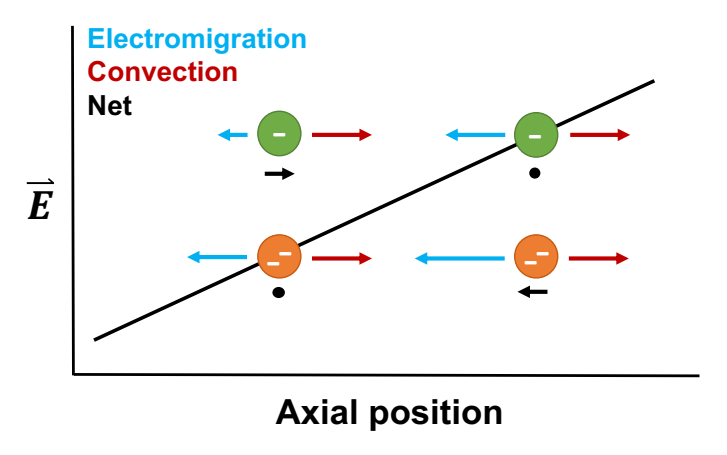
1. Introduction

The demands of clinical, environmental, and pharmaceutical applications have long driven the advancement of analytical techniques towards improved limits of detection (LOD), greater specificity, and decreased analysis time. Despite these efforts, low analyte concentration, limited sample volume, and the complexity of matrices still present major challenges and motivate the development of more advanced sample preparation. Lab-on-a-chip (LOC) devices integrate microto nanoscale fluidic structures with electrodes or chemically-modified surfaces to confer several distinct advantages including efficient handling of small volumes, rapid analysis, and access to surface-driven physical phenomena. In this context, electrokinetic forces are ideal for performing fluidic operations and for manipulating charged species and/or biological objects such as DNA, proteins, and cells.¹ Due to these features, several miniaturized or on-chip electrokinetic preconcentration techniques such as electric field gradient focusing (EFGF),²⁻⁶ field amplified sample stacking (FASS),⁷ isoelectric focusing (IEF),⁸ isotachophoresis (ITP),^{9,10} dynamic field

gradient focusing (DFGF),² and temperature gradient focusing (TGF)^{11–13} have been developed for analyte preconcentration and/or separation. These methods share an ability to achieve an abrupt change in the velocity of the analyte at a defined spatial location along an electric field. For example, in ITP, charged analytes are introduced between leading and trailing electrolyte (LE and TE), which have co-ions of relative high and low mobility, respectively. The mismatch in mobilities dictates low and high electric field strengths in respective channel segments given the condition that continuity in ionic current must be maintained. Analytes are separated along this electric field gradient into discrete bands based on their electrophoretic mobilities. Importantly, the electrophoretic mobility of an analyte must be less than that of the co-ion of the LE and greater than that of a TE, and therefore, must be known in advance. Ion concentration polarization focusing (ICPF) is among the most recently developed of these techniques and is used for both analyte enrichment and separation. In ICPF, charged analytes are focused along a steep gradient in electric field strength in the presence of opposing fluid flow. ICPF allows for continuous sample supply and perpetually generates and maintains a steep gradient in background electrolyte (BGE) concentration, thus improving the preconcentration factor for low abundance analytes.¹⁴

Ion concentration polarization (ICP) is the simultaneous enrichment and depletion of ions at opposing ends of an ion permselective structure when an electrical field is applied across it. Leinweber and Tallarek were first to quantify ICP in a packed mesoporous bead bed in a capillary.¹⁵ In microfluidic systems, Pu et al. showed the first reported visualization of CP near nanochannels and presented a qualitative model describing it.¹⁶ Since then, multiple research groups have expanded the application of ICP, and further characterized it as a means for control over species transport. Ion depletion is particularly important because it leads to a localized increase in solution resistance, which by Ohm's Law, enhances the electric field strength. The

resulting electric field gradients at the boundary of this ion depleted zone (IDZ) have been employed extensively for focusing and separation of charged analytes in the presence of counterflow. If two species with distinct electrophoretic mobilities are introduced into the system (for example two different fluorescent dyes¹⁷ or phosphorylated and unphosphorylated substrates in an enzymatic assay), ¹⁸ each species will be focused at a distinct axial location (**Scheme 1**).



Scheme 1. Illustration of electrokinetic focusing of two anionic species having high (orange) and low (green) electrophoretic mobilities along a gradient in electric field strength. The anions have a convective velocity, from left to right, that is constant as a function of axial position. Their electromigratory velocities (from right to left) are the product of the distinct electrophoretic mobility of each anion as well as the sign and magnitude of the electric field at each location. Therefore, for each anion, there is a position along the electric field gradient at which the net velocity is zero.

Separate reviews provide an account of the theoretical and experimental advances in ICP, ^{19–21} including various applications. ^{14,22} Specifically, ICP has been leveraged for desalination, ^{23–26} enrichment and separation of trace analytes ²² and bioparticles, ²⁷ cellular dielectrophoresis, ²⁸ regeneration of sensing substrates, ²⁹ and biological assays. ^{18,30}

Besides analyte focusing and separation, another important application of the ICP phenomenon is micromixing. Mixing solutions at the microscale is slow and often inefficient due to their operation in a laminar flow regime, where mixing is governed by diffusion. The

electroconvection generated by ICP near ion selective membranes or nanochannels can be used to mix solutions in neighboring flow laminae. Several active and passive micromixer platforms have been developed for lab-on-chip applications.^{31–33}

Faradaic ion concentration polarization (fICP) (called bipolar electrode (BPE) focusing when performed using bipolar electrochemistry) is analogous to ICP with the exception that local ion concentration is controlled electrochemically via charge transfer reactions at an electrode.^{34–36} BPE focusing has been used for both enrichment and separation of charged analytes.³⁵ Recently, fICP has been demonstrated as an alternative to conventional ICP for enrichment of charged species for analysis,^{34,35,37} redirection of microbeads,³⁸ and dielectrophoresis.²⁸ Techniques that rely on electric field gradients formed by ICP and fICP have shared advantages and limitations, and thus, both will be discussed in this tutorial review.

Despite tremendous advancements in ICP and fICP, some aspects remain challenging. For example, the extension of focusing to neutral (uncharged) species, improvement of volumetric throughput, integration with downstream analysis, application to complex media (e.g., plasma, blood), and the development of strategies to decrease fluidic instability within the IDZ are active areas of research.

In this tutorial review, we briefly introduce physical and chemical aspects of ICP including its theoretical background, primary configurations of the fluidic channel(s) and electric field, the origin of fluidic instability and strategies to mitigate it, propagation of the IDZ boundary (and of the focused analyte bands), and dynamic local pH changes. Next, we describe practical aspects of ICP including methods of device fabrication, prevalent ion selective materials and methods of incorporating them into devices, the influence of sample composition on the selection of device configuration and on the efficiency of focusing, and analyte encapsulation to 'lock in' pre-

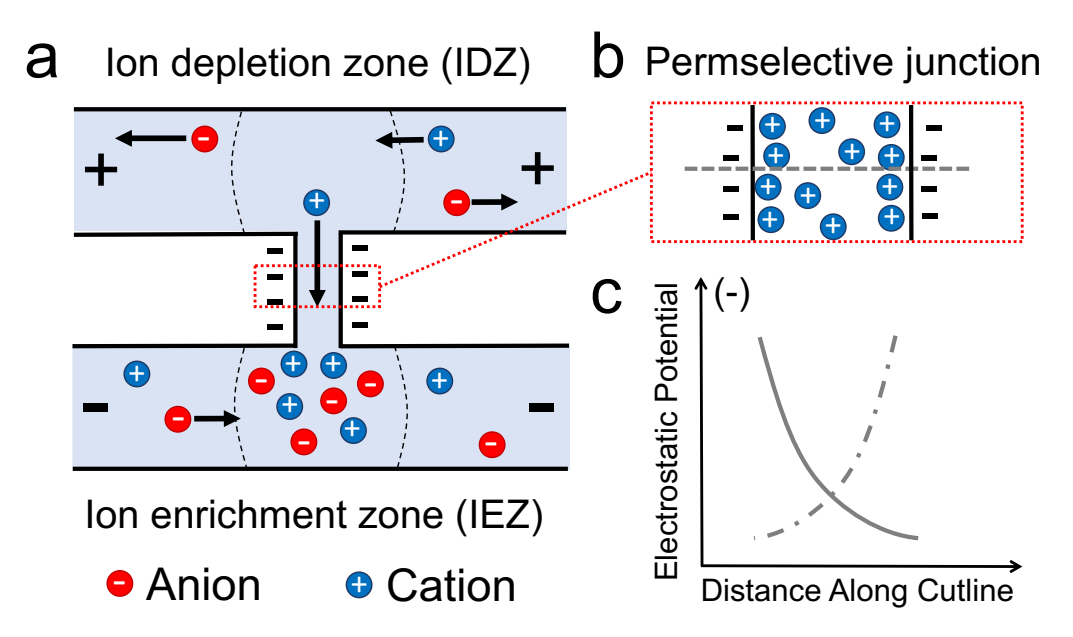
enrichment for off-chip analysis. We further address methods for on-chip analysis, which primarily leverage ICP to control mass transport to/from chemically-modified surfaces. We highlight recent advancements such as multi-staged concentrators, micellar ICPF and an approach for in-droplet enrichment. Lastly, we include a summary of tips and tricks to utilize ICP effectively within its practical and theoretical limits for focusing charged and neutral species.

2. Fundamental aspects of ICP

In this section, we summarize the key physical and chemical aspects of ICP. We first discuss the mechanisms by which selective ion transport (Donnan exclusion) and, alternatively, faradaic reactions lead to ion depletion in an extended space charge region (the IDZ). Second, we summarize device and electrode configurations employed to achieve the requisite electric field across both the ion selective structure and the microfluidic compartment in which electrokinetic focusing occurs. Third, the transport phenomena that contribute to the formation of disruptive vortex flow and strategies to dampen their effects are described. Next, experimental regimes that promote upstream propagation of the IDZ boundary, which in many applications is undesirable, are delineated, and reported strategies to prevent propagation are discussed. Finally, we describe the processes leading to spatiotemporal shifts in pH, their impact on the sample, and how to control their location and magnitude.

2.1. Mechanism of ICP

ICP occurs when a majority of ionic current is selectively carried by either cations or anions between two compartments interconnected by an ion permselective structure when a voltage bias is applied. 14,19 **Scheme 2a** is an illustration of a nanoscale junction, with fixed negative surface sites along its walls, that separates two microfluidic compartments. When a voltage bias is applied across the junction, as shown, cations are selectively transported out of the anodic compartment. Anions migrate towards the anodic driving electrodes, leading to formation of an IDZ in which ion concentration approaches zero. In the cathodic compartment, anions migrate to the junction but are unable to enter, and cations accumulate there to maintain electroneutrality. These processes lead to ion accumulation, thus creating an ion enriched zone (IEZ). A key point is that the low ionic conductivity in the IDZ results in localized electric field enhancement that drives even more rapid depletion, resulting in growth and propagation of the IDZ.



Scheme 2. a) Illustration of IDZ and IEZ formation near a nanoscale junction spanning two microfluidic compartments; b) illustration of the electrical double layers at the negatively charged walls of the nanojunction; and c) a schematic plot of the electrostatic potential as a function of distance from each wall. In this illustration, the electrical double layers overlap, and therefore, the electrostatic potential at every location within the junction is more negative than that of the bulk solution.

Because of this mechanism of permselectivity by Donnan exclusion, the ratio of the channel/pore radius to the Debye length of the electrical double layer (EDL) is a key parameter impacting the initiation of ICP and propagation of the IDZ.¹⁹ An EDL forms at any solid-liquid interface and is on the order of a few nanometers (< 10 nm) in a symmetric electrolyte at a concentration greater than 1.0 mM. If the channel wall is negatively charged, the electrical potential at the wall will be more negative than that of the bulk solution (**Scheme 2b**). If two such walls are in close proximity to each other, the EDLs will overlap and the electric potential in the center of the channel will not reach that of the bulk solution (**Scheme 2c**). A non-zero voltage bias will drive selective transport of cations through the junction. Practically, this condition is satisfied when the ratio of channel/pore height to the Debye length is unity or less ($h/\lambda_d \le 1$, where h is the height of the channel/pore and λ_d is the Debye length), thus implying that the ICP phenomenon is limited to nanochannels with a critical length on the order of 10 nm or less.

However, Kim et al. demonstrated that strong ICP effects can be achieved with non-overlapped EDLs.³⁹ They observed ICP at nanochannel with a critical dimension of 40 nm in the presence of an electrolyte concentration of 15 mM, which corresponds to a 3 nm-thick EDL. Additionally, Jacobson and coworkers showed that strong ICP effects can be achieved even with non-overlapped EDLs.⁴⁰ Using a poly(ethylene terephthalate) (PET) membrane with track-etched conical nanopores sandwiched between two PDMS microchannels, they showed that despite an estimated EDL thickness of 1-3 nm in a nanopore having a diameter of 130 nm, ICP occurred ($h/\lambda_d \approx 100$). To investigate the ion selective transport mechanism, these authors measured and compared the conductivities of the buffer in the bulk solution, in the microchannel and in the nanopores while varying the concentration of the buffer. Their results demonstrated that the bulk and microchannel conductivities were directly proportional to each other over the entire buffer

concentration range, while the nanopore conductivities exhibited a positive deviation at low buffer concentration. This greater than expected conductivity is due to the increased surface-to-volume ratio in the nanopore, which leads to an increased contribution to the nanopore conductivity from the surface charge. This result suggests that under the condition that ion conduction along the surface of the nanopore is a major contributor to the overall current, ICP will occur.

Zangle et al. coupled theoretical and experimental studies to investigate the relationship between surface and bulk conductance in the generation of ICP. They concluded that concentration polarization depends primarily on a nondimensional parameter called the Dukhin number (Du) and not strictly on the ratio of channel/pore radius to Debye length. ^{19,41} Du is the ratio of the surface (G_{σ}) to bulk (G_b) conductance:

$$Du = G_{\sigma}/G_{b}$$

Mani et al.,⁴¹ Zangle et al.,⁴² and Kim et al.⁴³ further used the inverse Dukhin number (1/Du), to characterize concentration polarization. The 1/Du relates the number of ions in the bulk to the number of ions associated with the EDL.

$$1/Du \approx Fhzc_0/\sigma$$
, where

F is the Faraday constant, h is channel or pore height, z is valence of a symmetric electrolyte, c_0 is bulk concentration of electrolyte ions, and σ is surface charge density. Strong concentration polarization effects have been demonstrated for systems where $Fhzc_0/\sigma \ll 1$. In other words, for ICP to occur, selective conduction of counter-ions along the surface must greatly exceed non-selective bulk conduction, and this ratio depends on the availability of charge carriers to each current path.

Several studies have measured both bulk and ion selective currents, as a function of applied voltage, and have related them to the rate of ion depletion and IDZ propagation. The depletion zone length increases as the applied voltage bias and the current through a permselective junction increase. Most commonly reported currents through a cation selective membrane in ICP systems are within a range of tens of nA for small channel geometries (with channel cross sectional area of $400 \, \mu m^2$). The several studies have measured both bulk and ion selective currents, as a function of applied voltage, and have related them to the rate of ion depletion and IDZ propagation. The depletion and IDZ propagation.

2.2. Mechanism of faradaic ICP

Faradaic reactions can be used to generate ion depleted and enriched zones that are analogous to those resulting from ICP at permselective junctions. For example, neutralization of ions of the BGE at an electrode leads to their depletion. In the application of faradaic ICP (fICP), these reactions are most commonly facilitated by a BPE. A BPE is a conductive material, that is not directly connected to an external power supply, and thus is free to float to an equilibrium potential. The application of a potential bias (ΔU_{tot}) is applied across the electrolyte solution in contact with the BPE, an interfacial potential difference will develop between the BPE (U_{BPE}) and the solution at each of its ends (**Scheme 3a**). If the total potential dropped across the BPE (ΔU_{BPE}) is sufficiently large, the electrochemical overpotentials, η_a and η_c , will drive anodic and cathodic reactions that are electrically coupled through the BPE. **Scheme 3b** (top view) and **Scheme 3c** (cross-sectional side view) illustrate a thin film BPE in contact with two parallel microchannels. Reduction of a cation to a neutral product at the BPE cathode (top channel, **Scheme 3b**) results in a decrease in local ion concentration. This process is coupled to an oxidation reaction at the BPE anode (bottom channel). As depicted here, the oxidation of a neutral compound generates a cation,

and concurrent inward migration of anions to charge pair with these cations leads to a local increase in ionic strength (an IEZ). This combined process is analogous to selective cation transport.

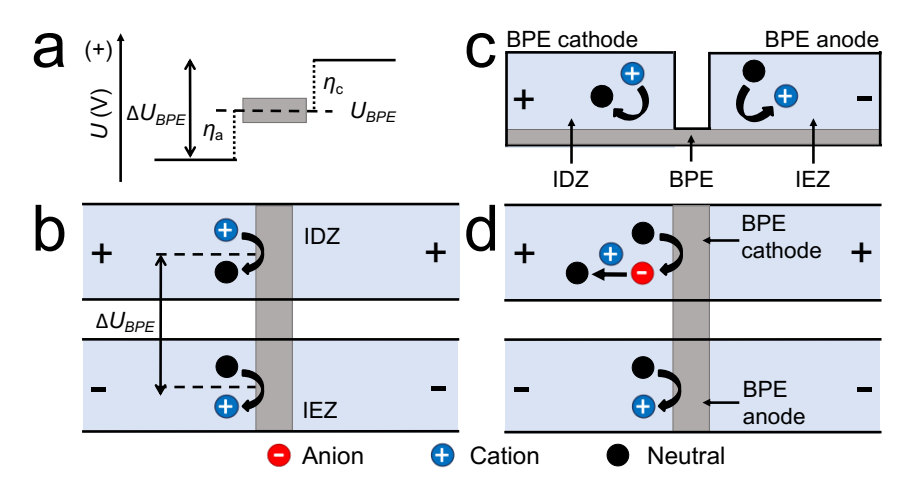
Scheme 3d depicts an alternative route to fICP involving acid-base neutralization of buffer ions.

Here, water is reduced to generate OH⁻ (red circle, top, Scheme 3d), which accepts a proton from a buffer cation (blue circle, e.g., TrisH⁺) to generate a neutral species (black circle, e.g., Tris), thus resulting in a local decrease in ionic strength and creation of an IDZ.

Note that for fICP, the degree of selectivity (similar in concept to Du in ICP) is the ratio of the faradaic current leading to ion depletion to the bulk ionic current. Therefore, for a system in which the reaction proceeds with 100% faradaic efficiency and in which all current is passed through the electrode that drives CP, there is perfect selectivity (analogous to infinite Du). An important limitation of fICP, however, is that faradaic processes are not simply charge selective – they are also species selective, depleting one type of cation (e.g., TrisH⁺) while leaving another (e.g., Na⁺) untouched. The resulting partial depletion is analogous to a low Du. This characteristic presents a major challenge for fICP in complex media, and therefore, a key area for growth in fICP is the identification of electrochemical processes that deplete major charge carriers in systems of interest.

When designing a strategy for fICP, there are several key factors to consider. First, it is not required that the electrode be a BPE – any electrode in a confined volume that drives reactions leading to significant removal of ionic charge carriers of the BGE can facilitate the development of an IDZ. Second, the reactions can be either a faradaic oxidation or reduction and can act either directly or indirectly on the ions of the BGE. For example, at an anode, the generation of protons by water oxidation can drive ion depletion indirectly via the neutralization of a buffer anion. Such neutralization can be complete (e.g., CH₃COO⁻ to CH₃COOH) or partial (e.g., HPO₄²⁻ to H₂PO₄⁻

).⁵¹ However, complete neutralization leads to a more dramatic decrease in local ionic strength, and therefore, to greater electric field enhancement within the IDZ. Finally, the sign of the excess charge on the electrode determines the direction of the electric field gradient, and therefore, dictates which sign of analyte (cationic or anionic) can be focused. Anions are focused against a counter flow by repulsion from an IDZ generated at a cathode (and vice versa).



Scheme 3. a) Schematic plot of the electrostatic potential (U) of the electrolyte solution and the BPE (U_{BPE}) , an equipotential object, along the dashed cutline in (c). In an externally applied field, an interfacial potential difference develops between the BPE and the solution at each of its ends. b) Top view and c) cross-sectional side view schematics of a thin film BPE in contact with two parallel microchannels. Faradaic reactions occur at the BPE cathode and anode, impacting the concentration of cationic (blue circles) and neutral (black circles) species in each compartment. d) Schematic illustration of the device shown in (b), in which an alternative mechanism leads to ion depletion. Faradaic production of anionic species (red circle) leads to depletion of a cations (blue circle) by a following reaction.

2.3. Electric and flow fields that drive ICPF

This section focuses on the aspects of the applied electric field and fluid flow that contribute to the rate of ion depletion and the electric field distribution – especially, its magnitude and slope where focusing occurs – and to the rate of convection. In most cases, initiation of ICP requires a voltage bias across an ion permselective junction (E_I) .²⁰ A peak in electric field strength

develops at the location where ion depletion is the greatest and forms an electric field gradient extending up to several hundred microns to the edge of the IDZ (**Figure 1**). See Hlushkou et al. investigated ICP at hydrogel membranes with varying surface charge densities and the associated electric field formed upon applying a potential bias. **Figure 1a** depicts a single-channel device employed in this study to obtain both numerical and experimental results. At the channel midpoint, a fixed hydrogel plug connects the anodic and the cathodic compartment of the microchannel. Species transport was governed by electroosmosis and electrophoresis. There is convection along the microchannel from left to right (**Figure 1**), and the fluid flows through the hydrogel. A charged hydrogel can drive EOF, acting as a pump. **Figure 1b** shows the result of numerical simulations of the electric field near charged ($c_{fix} = c_{res}$, and $c_{fix} = 0.1c_{res}$) and uncharged membranes ($c_{fix} = 0$). Focusing of a charged species can be achieved at an axial location along this field gradient, at which the convective and electromigratory velocities of that species are equal in magnitude and opposite in direction. The second content of the result of the species are equal in magnitude and opposite in direction.

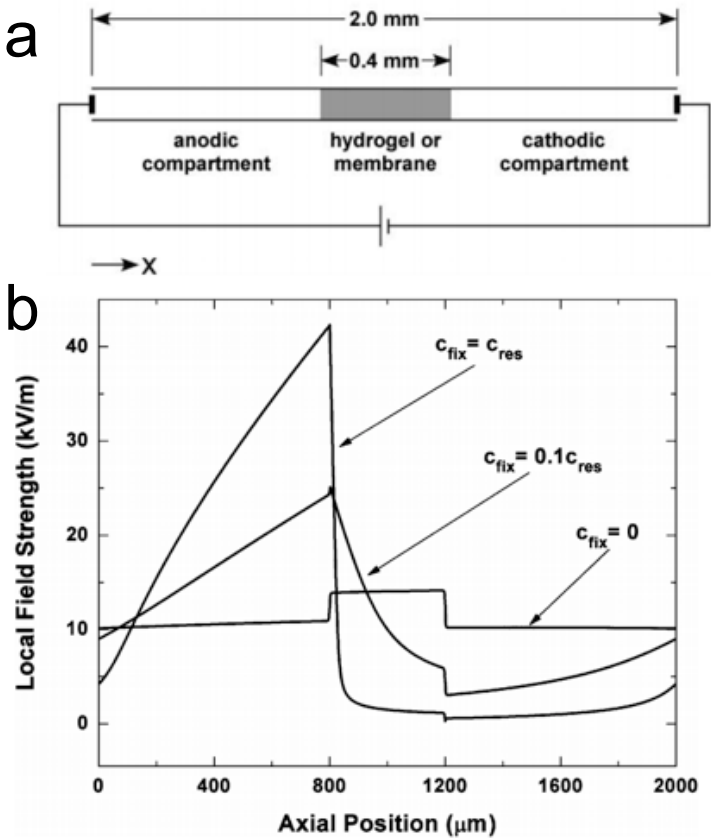


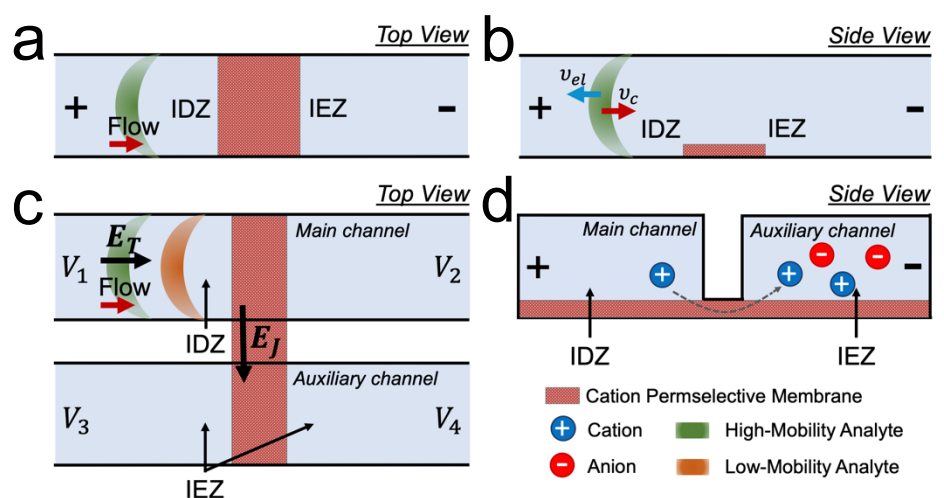
Figure 1. a) Schematic illustration of the system used for analyte concentration enrichment in a microfluidic channel containing a fixed nanoporous (anionic or neutral) membrane. b) Numerical simulation of the steady-state distribution of the local electrical field strength for an externally applied field of 11.1 kV m⁻¹. Three cases are shown, in which the membrane was assigned a negative fixed charge of uniform volume density of $c_{fix} = 0$ (neutral), $c_{fix} = 0.1c_{res}$ (weakly charged), and $c_{fix} = c_{res}$ (highly charged). c_{res} is the concentration of the BGE in the reservoir. The membrane occupies the region x = 800-1200 μm. Illustration reproduced from ref. [52] with permission.

Kim et al. investigated the current and voltage requirements for inducing ICP in a single microfluidic channel having a surface patterned *Nafion* membrane film along a segment of the channel floor.⁵³ They found that if cation flux through the patterned membrane was larger than that through the bulk solution (high Du), then ICP occurred. **Scheme 4a** and **4b** illustrate a top view and cross sectional side view of a single microchannel with an embedded membrane, where V_1 and V_2 are the voltages applied in the microchannel reservoirs. Fluid flow is from left to right,

and the green band represents a plug of enriched anionic analyte upstream of the membrane. The convective and electrophoretic components of their velocities are indicated as v_c and v_{el} , respectively. In the device employed by Kim et al., the channel was 200 μ m wide by 20 μ m tall and with a membrane, that extended 200 µm along the channel length, spanning the channel centrally. In this configuration, initiation of ICP required 50 V/cm electric field. In a subsequent publication with a similar device geometry, this same group developed a model to characterize the influence of several experimental parameters on the enrichment factor (EF) in this single-channel ICP device.⁵⁴ EF is calculated as the maximum localized concentration observed in the enriched plug of analyte divided by its initial concentration in the sample. These parameters included the voltage bias (V+), electrophoretic mobility of the analyte (μ_{ep}) , the charge density in the membrane (σ) , and the electrolyte concentration (c_0) . The authors concluded that, although single-channel ICP devices are simple to fabricate and to operate (two driving electrodes, no auxiliary channel), they are limited to applications with low electrolyte concentrations (≤ 0.1 mM) for sufficiently high Du. Additionally, at a spatially averaged electric field strength of 50.0 V cm⁻¹ or higher, the Nafion membrane (100 μ m long and 2 μ m thick) was damaged and degraded within 15 min.

In **Scheme 4c** and **4d**, two fluid filled compartments are connected solely by an ion selective junction. Such a system can be achieved experimentally by contacting two microfluidic channels with a cation selective membrane (top view, **Scheme 4c**, and cross-sectional side view, **Scheme 4d**). **Scheme 4c** depicts two anionic analytes with distinct mobilities as focused bands upstream of the membrane in the main (anodic) channel. This dual-channel configuration allows the operator to tune the components of the electric field normal to the membrane (E_I) and tangential to fluid flow (E_T) independently. Therefore, the current through the membrane can be kept below the threshold for damage while maintaining tight focusing. More specifically, when $V_1 > V_2$

(Scheme 4c) the magnitude of E_T is increased, leading to increased migration velocity and higher EOF-driven flux of the analyte to the enriched band, thereby resulting in greater enrichment.⁵⁵ In such a configuration, it is typical that $V_3 = V_4 \le V_2$ such that $E_I > 0$.



Scheme 4. a) Top view and b) side view illustrations of a single-channel device with an embedded membrane. An analyte (green) is focused upstream of the membrane by a balance of electrophoretic and convective forces. c) Top view and d) side view illustrations of a dual-channel device, in which two parallel microfluidic channels are interconnected by an ion permselective membrane (e.g., *Nafion*). Two analytes (green and yellow) are focused at distinct axial locations determined by their individual electrophoretic mobilities.

This dual-channel configuration has been used to simultaneously preconcentrate and separate multiple species that have distinct electrophoretic mobilities. This approach is especially effective for analysis of biological targets, for which a biorecognition event, such as binding, chemical modification, or cleavage, leads to a shift in mobility. Recent examples include the detection of 1) a protein by the separation of bound and free aptamers,⁵⁶ 2) a kinase through discrimination of phosphorylated and unphosphorylated substrates,¹⁸ and 3) a specific DNA sequence by its complexation to Cas9.^{57–59} A universal strategy to improve resolution that arose from these methods is the inclusion of spacer molecules (here, peptides comprised of neutral and acidic residues) having mobilities intermediate to those of separands. When enriched to a

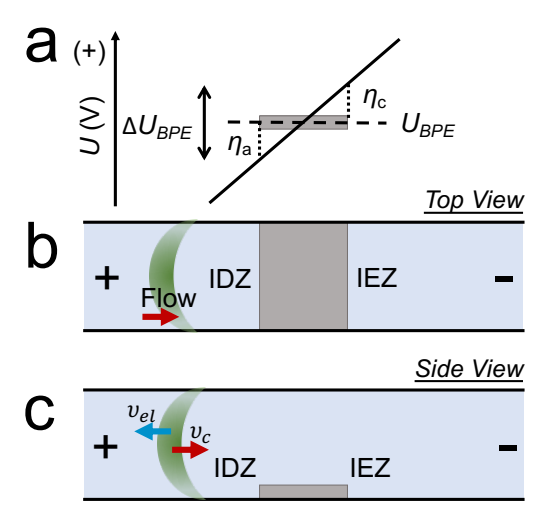
concentration near that of the BGE, the spacers generated steps in the electric field gradient that push apart analytes that focus at higher and lower field strengths.¹⁸

fICP similarly has been demonstrated in both single- and dual-channel configurations. A single-channel configuration for fICP, in which the entire BPE is in one channel, has been employed for focusing of either anions or cations (**Scheme 5a,b**)^{34–36} and for separation of multiple analytes.⁶⁰ Application of voltage bias, ΔU_{tot} , across a single microchannel of length l_{chan} with embedded BPE results in an electric field with a constant value of $E \approx \Delta U_{tot}/l_{chan}$. If there is a sufficient potential dropped across the solution above a BPE (of length, l_{elec}), faradaic electrochemical reactions will occur at the poles of the BPE. Electrochemical reactions will occur when the fraction of ΔU_{tot} dropped over the length of the BPE (approximated by $\Delta U_{BPE} \approx \Delta U_{tot} \times l_{elec}/l_{chan}$ and depicted in **Scheme 5c**) exceeds that required to drive a reduction reaction at the cathodic pole and an oxidation at the anodic pole.⁵¹ In other words, ΔU_{BPE} must exceed the difference in onset potential between the two electrically coupled reactions. By employing a single-channel configuration, small anionic dyes were enriched up to ~500 fold within 400 s.⁶⁰

It has been reported that during fICP in a device configured such that both ends of the BPE lie in a single microchannel, a majority of current flows through the BPE and not through the bulk solution. Importantly, approximately 80% of the total current is diverted through the BPE. For example, at a total current of 328 nA, the current through the BPE was reported to be 271 nA. 36 This high ratio of a faradaic current (that selectively depletes one sign of charge carrier) to bulk current is analogous to a high Du in ICP. This finding is important because it has allowed for focusing in devices lacking nanoscale, or even low microscale, dimensions.

Scheme 3 depicts a BPE in contact with two microchannels. Such dual-channel focusing offers multiple advantages. First, the ability to select either cathodic or anodic reactions leading to

ion depletion provides a route to simultaneous enrichment of both cations and anions in the same device. For example, dual IDZs form with indirect neutralization of TrisH⁺ and CH₃COO⁻ at the BPE cathode and anode, respectively.³⁵ Second, E_J and E_T are controlled independently, thereby preventing damage to the electrode caused by Joule heating or by redox reactions of the electrode material itself. A higher E_T allows for an enhanced rate of enrichment via more rapid transport of the analyte to the IDZ boundary and tighter focusing.^{34,35} Using dual-channel focusing, up to 143,000-fold EF within 33 min (71-fold/s) of a tracer dye was reported.³⁵



Scheme 5. a) Top view and b) side view illustration of a single-channel fICP device with an embedded BPE. c) Schematic plot of electrostatic potential of the electrolyte solution as a function of axial position along the channel. The potential of the BPE is intermediate to that of the solution it contacts. This simplified schematic assumes no impact of the BPE on the solution potential.

In practice, convection is achieved by electroosmotic flow (EOF), pressure-driven flow (induced by gravity or a syringe pump), or a combination of both. During focusing of a charged species, convection plays the role of carrying it from the inlet reservoir to the location at which opposing electromigration is sufficiently strong to balance it. Therefore, the convective velocity of the species must exceed its spatially averaged electromigratory velocity. For example, a small molecule with an electrophoretic mobility (μ_{ep}) of 3.0 x 10⁻⁸ m²/V·s in a 5 kV/m electric field, will

have an electrophoretic velocity of 1.5 x 10^{-4} m/s (150 μ m/s). In the IDZ, the electric field strength can be 10-fold greater (50 kV/m) than the average along the channel. Therefore, in the presence of electroosmotic flow (EOF) with a spatially averaged linear velocity of 500 μ m/s, the species described will be carried to the IDZ and focused at an axial location where the electric field reaches 16.7 kV/m. Native glass, silicon, and materials commonly employed in microfluidics such as polydimethylsiloxane (PDMS) have negatively charged surface groups (Si-O-) over a wide pH range (pK_a 4-6) leading to a surface charge on the order of 10 mC/m².⁶¹ The resulting negative zeta potential (ζ) drives EOF towards the cathodic driving electrode in the presence of a tangential electric field (E_T) . Note that ICPF of cationic analytes near an anion selective membrane would require an anodic EOF, which can be achieved by modifying the channel walls with a cationic coating. Where EOF alone drives convection, E_T is directly proportional to both convective and electromigratory velocities, and in general, a higher field strength leads to tighter focusing – the width of the analyte band is determined by how well these sequestering forces can counter diffusive broadening. However, E_T is practically limited by the onset of fluidic instability, which is discussed in detail in Sections 2.3 and 2.4.

The electroosmotic mobility (μ_{eo}) can vary considerably depending on the pH of the sample and the properties of the microchannel surface, and therefore, it is practical to dampen EOF with an uncharged surface coating (such as poly(ethylene glycol)-block-poly(propylene glycol)-block-poly(ethylene glycol) or Pluronic F108)^{62,63} and rely on pressure driven flow instead. However, note that the flow rates required for ICP are very low and therefore difficult to control with a syringe pump. Take for example the 500 μ m/s EOF described above. In a microchannel having typical dimensions (200 μ m x 50 μ m), the volumetric flow rate is only 5.0 nL/min. In the

absence of a pump that can stably deliver such a low flow rate, gravity-driven flow arising from a fluid height differential across the inlet and outlet reservoirs is often employed.

2.4. Secondary EOF or vortex flow

The efficiency of ICPF is limited by a strong secondary electroosmotic flow that develops within the IDZ, creating fluid vortices that cause unwanted mixing. Recently Nam et al. summarized key features of this fluidic instability.⁴⁷ The origin of this phenomenon is a sharp decline in the electrolyte concentration within the IDZ. The concentration of ionic charge carriers approaches zero at the limiting current,¹⁶ and the resulting decrease in electrical conductivity leads to a locally amplified electric field.⁶⁴ This high local electric field drives fast electrokinetic flow within the IDZ to transport sufficient ions to the junction to satisfy electroneutrality conditions.^{39,65} A mismatch in the local driving force for EOF inside versus outside of the IDZ leads to circulating (vortex) flow and results in disruption of concentration gradients. Therefore, the onset of vortices can be detected indirectly as a decrease in the electrical resistance of the IDZ and excursion of current above the limiting value (overlimiting behavior).

Prior to this more recent summary, several research groups proposed multiple mechanisms for fluidic instability. Zaltzman and Rubinstein experimentally investigated changes in current associated with fluidic instability. They found that current through an ion selective membrane increases linearly with increasing applied electric field (ohmic regime), until reaching a voltage-independent current limited by mass transport of ions through the depletion zone (limiting current regime). At still higher voltages, the onset of fluidic instability and mixing decreases resistance in the IDZ, leading to increased current through the nanoporous membrane (overlimiting current

regime).⁶⁶ They characterized the mechanism of this instability including contributions from thermal fluctuations,⁶⁷ non-equilibrium electroosmotic slip,⁶⁸ and electro-diffusio-convection.⁶⁶

Mani et al.⁴¹ and Park et al.⁶⁹ described factors affecting vortex formation near a nanojunction. These authors concluded that because the ratio of surface to bulk conductance depends on the cross-sectional area of the channel, the EOF profile is non-uniform across the microchannel-nanochannel interface. A local mismatch in EOF causes internal pressure gradients near the interface, thus creating vortices in the channel.

Recently, a more unified theory of the mechanisms contributing to overlimiting current was proposed. 70 Diffusion-limited transport to an ion selective membrane or to an electrode in a microchannel having charged walls was described using three mathematical models: 1. surface conduction (SC) by the excess counterions that screen the wall charge; 2. convection by EOF, which is driven by large electroosmotic slip in the depletion region on the sidewalls; and 3. electroosmotic instability (EOI) or fluid vortices. For the mathematical model, authors used symmetric electrolyte ($c_0 = 1.0$ mM), with microfluidic channel length L = 1.0 cm, surface charge of 50 mV, and channel height, H. The predicted mechanism for overlimiting current transitions were from SC to EOF at $H = 8.0 \mu m$, and from EOF to EOI at H = 0.4 mm. It was concluded that the SC mechanism dominates for very shallow channels, low ion concentration, and large surface charge, while EOF dominates in taller channels. Further, with increasing channel height, the dominant mechanism switches to EOI because a significant portion of the depleted solution is unaffected by the EOF. These result indicate that the dominant mechanism leading to overlimiting behavior and vortex formation can vary based on microfluidic channel dimensions and ionic strength.⁴⁷

Few experimental approaches have been developed to reduce the impact of vortex formation and fluid mixing on IDZ stability. Reducing the cross-sectional area of the main channel can lead to vortex flow suppression and IDZ zone stabilization. Kim et al. demonstrated that electroconvection can be suppressed by decreasing microchannel depth. Upon decreasing from 20 to 2 µm, the vortex size was constrained to this smaller depth, thus leading to less efficient fluid mixing and a more stable concentration gradient near the permselective membrane.³⁹ However, this decrease in depth, led to a 10-fold decrease in volumetric flow rate (Q) under the same linear flow velocity, thus detrimentally lowering device throughput.

Similarly, Kim et al. utilized geometric 'microfin' structures near the ion selective membrane to reduce the size of vortices and increase the stability of the IDZ boundary (**Figure 2**). These microfin structures served to promote SC (instead of EOI) and also physically suppressed the electrokinetic vortices, resulting in a stable IDZ boundary at high voltage (110 V), while maintaining high preconcentration efficiency of charged species and increasing the overall throughput (up to $Q = 4.0 \mu L min^{-1}$) of the microfluidic device.

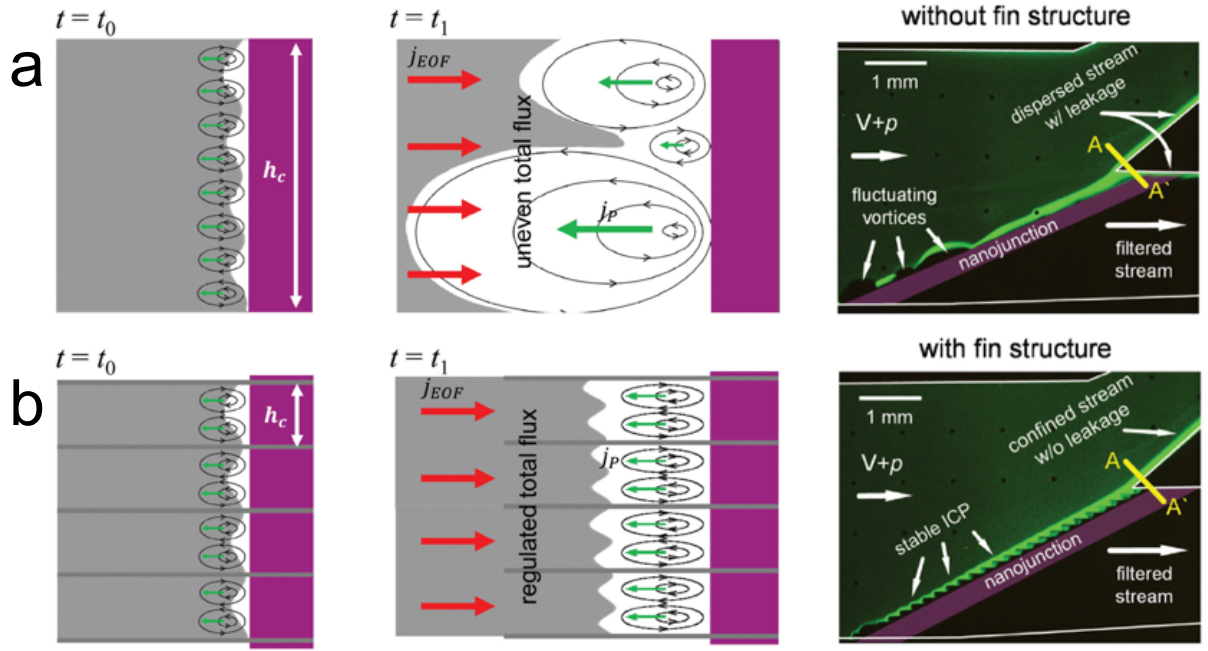


Figure 2. Schematics of vortex formation near a permselective membrane in each a device a) without and b) with the microfin structure. Here, h_c , j_{EOF} and j_P indicate the critical dimension, the ion flux by electroosmotic flow and back pressure due to vortex flow, respectively. Fluorescence micrographs of the high-throughput continuous ICP separator are shown at far right, for each device. Illustration in reproduced from ref. [46] with permission.

As an alternative to geometric restrictions, Kim et al. proposed that increased surface conduction can stabilize the vortex flow.⁴⁴ In their study, they achieved stable IDZ formation by artificially enhancing the surface charge of the channel by coating the highly conductive polymer (*Nafion*) inside the glass/PDMS microchannel. Highly conductive materials like *Nafion*, have surface charge in the range of 200-600 mC/m² (higher than glass). Therefore, they created an alternative current path (by enhanced SC) within the IDZ (**Figure 3b,c**). Consequently, the strong electrokinetic flow associated with the amplified electric field inside the IDZ was significantly suppressed.

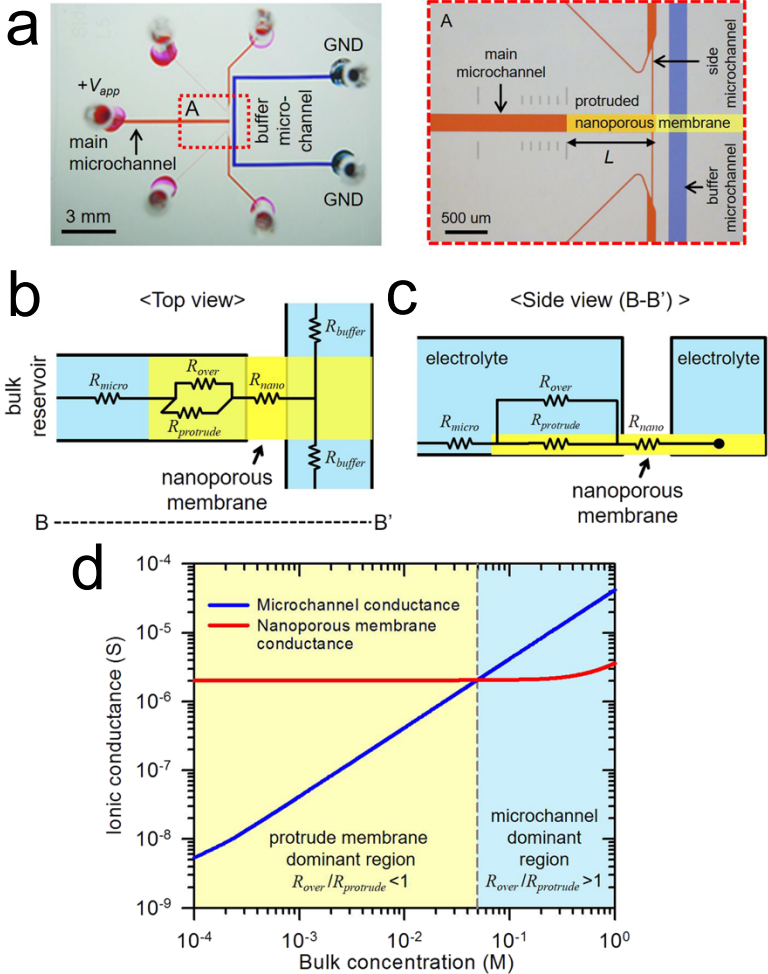


Figure 3. a) Top view image of the fabricated non-destructive cellular preconcentrator and microscopic view of the area indicated by the red box labelled A. L was the length that the nanoporous membrane protruded from the junction into the main microchannel. Schematics of b) top and c) side view of the proposed devices with equivalent electrical resistors (not to scale). d) Calculated ionic conductance of the microchannel and nanoporous membrane as a function of the bulk concentration of the electrolyte. Conduction of ions is dominated by the membrane at bulk concentrations below 4.0×10^{-2} M. Illustration reproduced from ref. [44] with permission.

A recent study by Valença et al revealed that microstructuring of an ion selective membrane facilitates ion transport to the membrane in the overlimiting regime, thereby reducing the need for EOI as a means of transport. The result is smaller fluid vortices.⁷¹ In this study, a caste-molding process was utilized to create 50 μ m-tall and 50, 100, 200, 400, or 800 μ m-long rectangular squarewave structures in the surface of a cation exchange membrane comprised of sulfonated poly ether

ether ketone (SPEEK). Chang and coworkers have shown that device design also plays an important role in determining the degree of instability.⁷² They found that a large ratio between the active areas of the driving electrode(s) and membrane leads to larger vortices. Therefore, designs that decrease this ratio and favor low current density are expected to exhibit greater fluidic stability.

2.5. Propagation of the IDZ boundary

Under certain conditions enrichment and depletion zones in a microfluidic system propagate outwards from the micro/nano-channel interface, creating shock waves.^{19,41} These shock waves are propagating boundaries between regions of channel with initial concentration $(c_{0,r})$ and regions where the concentration has been influenced by selective ion transport $(c_{0,r}^*)$. To be able to incorporate an analyte preconcentration step into a generic benchtop analysis or for point-of-care testing, the specific location of the concentrated analyte band within the microchannel must be known. However, due to propagation of the IDZ, controlling the location can be challenging.

Mani, Zangle, and Santiago developed and experimentally validated a computational model to characterize parameters that define propagating and non-propagating regimes. 19,41,42 They found, that these phenomena are governed by Du of the ion selective junction (here a nanochannel) and the mobility of the co-ion (e.g., anions for a negatively charged wall). As described previously, 1/Du represents the ratio of bulk to surface conductance. This parameter is proportional to nanochannel/pore height (h_n) and background electrolyte concentration $(c_{0,r})$ as supplied from the inlet reservoir and inversely proportional to the surface charge density (σ) . For computational purposes, they used non-dimensionalized concentration $(c_{0,r}^*h_n^*)$ and co-ion mobility (v_2^*) . They found that CP enrichment and depletion zones will propagate if the following condition is satisfied:

$$1/Du = c_{0,r}^* h_n^* < max \ (v_2^*, 2v_2^* - 1), \ where$$

$$c_{0,r}^* h_n^* = (v_1 z_1 - v_2 z_2) F h_n c_{0,r} / (-2v_1 \sigma), \ and$$

$$v_2^* = v_2 z_2 F \eta / \xi_n \varepsilon, \ where$$

 v_1 and v_2 are velocities of the counter and co-ion of the BGE, respectively, z_1 and z_2 are the valence of these ions, ξ_n is the zeta potential of the nanochannel, F is the Faraday constant, ε permittivity, and η is viscosity. In other words, a highly selective junction (defined as small 1/Du and $c_{0,r}^*h_n^*$) or a system in which the co-ion (which is repelled from the IDZ) is fast will yield propagation. By processing data from 56 sets of previously published experimental results and comparing them to the developed model, they observed that co-ion mobility values typically vary within two orders of magnitude (from 0.1 to 10) and thus, are not as influential as 1/Du, which extends over 4 orders of magnitude.

There are practical approaches that can be used to diminish the influence of propagation. For instance, the propagation of the depletion zone can be opposed by introduction of hydrodynamic flow or increase of EOF (by modifying the surface charge). Pressure driven flow is preferred because it is independently tunable. Undesirable "bursting" of the IDZ boundary occurs when the EOF overcomes the repulsive force of the IDZ.⁶⁴

Kwak et al. proposed an alternative method to control the propagation of the IDZ by confining preconcentration to a specific region regardless of the device operating conditions (time, applied voltage, ionic strength and pH).⁴⁵ To achieve this goal, they initiated ICP between two ion selective membranes (*Nafion*) located axially along a microchannel (**Figure 4**). These membranes were oppositely polarized such that an IEZ developed at the upstream junction and an IDZ at the downstream junction. This approach generated a preconcentrated plug of a model analyte in the 100 μm-gap between the membranes, thus simplifying in situ or in-line analysis.

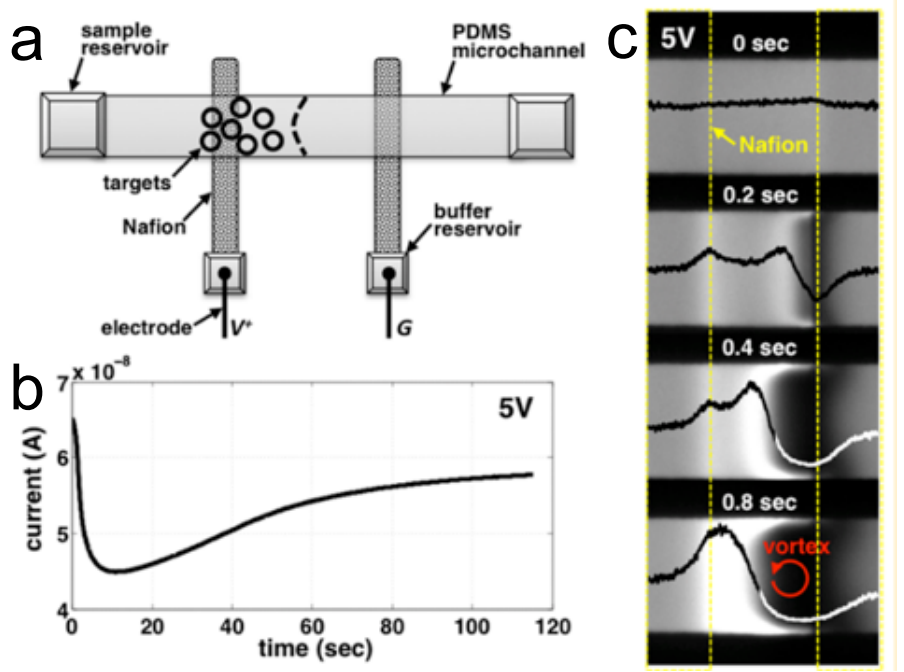


Figure 4. Schematic of a spatiotemporally defined preconcentrator. a) Analyte (black hollow circles) is preconcentrated between two *Nafion* strips, which are thin films, flow-patterned on the substrate; b) Current-time response obtained during performance of ICP at 5.0 V in this device; c) Fluorescence micrographs of the merged IEZ and IDZ between which an enriched band of a tracer dye develops. Illustration reproduced from ref. [45] with permission.

Vortex formation and ICP zone propagation can be decreased using capillarity ICP, an approach in which the capillary force of a permselective hydrogel, instead of an electric bias, spontaneously generates an IDZ.⁷³ Depletion occurs due to selective imbibition of counter ions from the sample solution into the hydrogel matrix, while its co-ions in the fluid are rejected from entering the hydrogel. Due to the difference in mechanism (e.g., passive transport of ions) electric field amplification does not occur inside the IDZ, and thus, no electrokinetic instability is observed. Despite the added stability, only a modest preconcentration rate of 100-fold/min was achieved for biomolecules, owing to a decrease in the magnitude of electrophoretic and convective forces available for focusing. Capillarity ICP holds promise for applications in which samples are

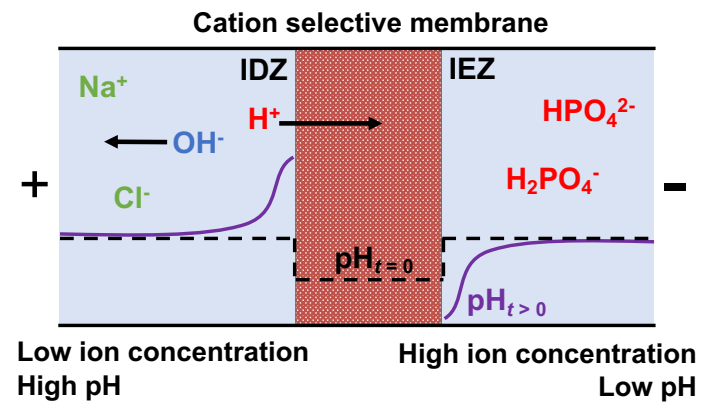
electrically sensitive (e.g., cells) or for point-of-care devices where high voltages are difficult to supply and only modest analyte preconcentration is needed.

2.6. Spatiotemporal pH dynamics near ion selective membranes and electrodes during ICP

Dynamic, localized changes in acid-base chemistry caused by permselectivity and ion accumulation and depletion at the ion selective structure may contribute significantly to nonlinear behaviors by affecting important system properties, such as analyte charge, local ionic strength and zeta potential of the channel walls, which are all coupled to pH. Further, the pH change may affect the kinetics of chemical reactions and directly interfere with molecular recognition and sensing reactions designated to occur near the ion selective feature. Often, ICP and fICP induce pH shifts on either side of the membrane or electrode as a result of H⁺/OH⁻ ion transport or production, respectively. The degree of change depends on key system parameters including buffer capacity, the pKa and density of charged surface moieties, and the magnitude of the current.

Mai et al. investigated the effect of ionic strength, electric field strength, and buffer composition on pH during CP at a negatively charged polyacrylamide (PAM⁻) membrane (**Scheme 6**).⁷⁴ The dual emission ratiometric fluorescent dye, carboxyseminaphthorhodafluor (SNARF), was used to monitor pH, while the degree of CP was ascertained based on the decrease in current (in a current vs. time plot) through the ion selective feature. The authors first investigated CP in two distinct buffer systems – 10.0 mM sodium phosphate buffer (PB, pH 7.5) and 10.0 mM phosphate buffer saline (PBS, with 150 mM NaCl, pH 7.5) under an applied electric field of 25 V/cm. A more rapid decrease in ionic current indicated stronger CP with lower ionic strength PB than with PBS. In one minute after applying the electric field, current through the ion selective

feature decreased by 75% in PB system, while in PBS they observed a 55% decrease. This outcome is expected based on the dominance of EDL conductance in the lower ionic strength buffer.



Scheme 6. Illustration of pH change near an ion selective membrane. During ICP, the pH profile evolves from its initial state (black dashed line) to develop a local maximum and minimum pH in regions near the membrane at later times (purple solid line). Illustration modified from ref. [74] with permission.

Further, the authors found that pH changes near the PAM⁻ structure were more pronounced in PBS than in PB alone. In PBS buffer, and under an applied electric field of 25 V/cm for 30 s, pH on the cathodic side of the PAM⁻ membrane decreased from 7.5 to 6. However, in PB, the pH was stable on the cathodic side. On the anodic side, an increase in pH to 8.5 was observed at the outer edge of the IDZ, at more than 500 μm away from the PAM⁻ membrane. Based on these results, it was concluded that higher ionic strength is correlated to a greater pH change. This result makes sense because a higher ionic strength will support greater overall current, thereby driving greater transport of H⁺ between the microfluidic compartments.

Finally, it was observed that the strength and rate of CP and the magnitude of local pH changes were positively correlated with applied electric field. As the field strength was increased, the initial current was higher and decayed more rapidly to its limiting value. These higher currents drive more rapid flux of protons through the membrane supporting greater excursions in pH.^{74,75}

Andersen et al. further developed a mathematical model to help predict and engineer pH dynamics that can be essential to the performance of ICP systems.⁷⁶

Similarly, the driving electrodes can facilitate electrochemical reactions that influence pH. Recently, Kim and co-workers demonstrated how electrode material and exposed area contribute to this effect. First, they compared Ag/AgCl electrodes with large (26.9 mm²) and small (0.2 mm²) electroactive area. Significant pH change was observed only at the small area electrode due to the high current density and resulting Cl⁻ depletion at the anode. Since the supply of Cl⁻ limited the oxidation of Ag to AgCl, water oxidation dominated instead, leading to decreased pH. These results were also compared to those obtained using Pt electrodes, where electrode area showed no significant influence on pH, because water oxidation was the only available reaction. Given these findings, selection of electrode materials, dimensions, and reactions is of critical importance for pH sensitive samples (e.g., proteins).

While these publications seek to prevent pH excursions in ICP, a stable pH gradient is useful for several applications, such as microbioreactions, and biomolecular separations. To take advantage of this feature of ICP, Cheng et al. developed a microscale pH actuator platform for pH regulation in a microchamber.⁷⁸ A controlled change in the pH of the BGE was achieved by injecting excess H⁺ or OH⁻ ions produced by field-enhanced water dissociation at the membrane upon application of a voltage bias. A stable pH gradient produced in this way was used to separate protein mixtures based on their isoelectric points.⁷⁹

3. Practical aspects of implementing ICP-based techniques

In this section, we summarize the key practical aspects of ICP. We first discuss the most commonly used device designs and fabrication methods for ICP-based techniques. Second, we provide a brief overview of materials that have been used to achieve selective ion transport. Third, we discuss the key aspects of sample composition, including analyte and electrolyte concentrations and mobilities, that dictate the limit of enrichment by one of two mechanisms (e.g., based on electrokinetics or electroneutrality). Further, we introduce additives that can be used to achieve ICP-based enrichment of neutral (uncharged) species. Finally, we give an overview of methods to encapsulate the preconcentrated analyte plug to prevent it from dispersing once the electric field is removed, thereby preserving it for further on- or off- chip analysis.

3.1. Device design and fabrication methods

There have been several reviews published describing microfluidic chip materials and fabrication. So Silicon, glass, elastomers, thermoplastics, and paper are used for fabricating microfluidic devices. Two-dimensional (2D) microfluidic systems are commonly used to investigate and demonstrate ICP phenomena. More advanced systems with multiple layers, valves and sensors require complex fabrication techniques (layer stacking, 3D printing), and are therefore used less frequently for fundamental studies.

Soft lithography is one of the most commonly used methods for 2D microfluidic device fabrication. Briefly, in soft lithography a master mold is fabricated by patterning a photoresist film on a Si substrate with a high-resolution photomask (lateral resolution approximately 10 µm for a printed mask and 500 nm for a chrome mask). This master mold is used to create a replica in a thermoplastic, by embossing, or in an elastomer, by cast molding. Polydimethylsiloxane (PDMS)

is a frequently used elastomer for microdevice fabrication due to its high thermal stability (stable below 400°C),⁸¹ elasticity, optical transparency, and ability to seal with itself (stacking) or a glass slide after plasma treatment.⁸² PDMS devices are disadvantaged by ready adsorption of small hydrophobic molecules and biomolecules onto channel walls, thereby making quantification of enrichment and separation by ICP a challenge. This problem can be partially addressed by modifying the channel walls to increase hydrophilicity – for example, PDMS can be reversibly coated with a block copolymer such as Pluronic F108 or F127, which are comprised of two ethylene glycol segments flanking polypropylene glycol.⁵³ The impact of such coatings on zeta potential on the channel walls and other device materials must be considered. For example, Pluronic dampens EOF, thereby requiring supplementation with pressure driven flow when convection is needed.

Three-dimensional microfluidic devices (3D) are fabricated by stacking multiple PDMS layers.²⁵ Out-of-plane or three-dimensional device designs have allowed large contact area between the sample solution and the membrane, thereby supporting increased volumetric throughput (up to 20 µL min⁻¹),²⁵ higher enrichment factors,⁸³ and better interfacing with downstream analysis.⁸⁴ 3D printing a thermoplastic material circumvents the need for high resolution photomasks, multilayer alignment, timed exposures, or development.⁸⁵ However, lower lateral resolution (about 25 µm)⁸⁶ and greater surface roughness restrict its applications in ICP.⁸⁷ Additionally, the development of thermoplastic materials that would be comparable in stability, elasticity and transparency with PDMS is still ongoing.

Paper microfluidic devices have a relative advantage for point-of-care applications due to their simplicity, low cost, and ease of fabrication.^{88–91} To fabricate paper-based ICP devices, channel designs are printed using wax to define walls. An ion selective feature is incorporated by

impregnating the paper with a conductive ink or resin solution. Currently, several groups have reported enrichment of low abundance analytes from 60-fold^{92,93} to 1000-fold⁹⁴ in paper by ICP, and 500-fold by fICP.⁹⁰

Several configurations of the driving electrodes, fluidic channels and ion selective features have been reported.²² Choice of device design and ion selective feature is governed by the application. Frequently, only one ion selective membrane or electrode is used to generate an IDZ in a microfluidic device. However, there is precedent for dual membrane configurations, in which a voltage bias applied across the membranes in series generates a neighboring IDZ and IEZ.⁴⁵ This format has been further employed to prevent propagation of the IDZ in paper fluidics and to achieve CP in water-in-oil droplets.⁹⁵ Also, ion selective membrane coated electrodes have been used for unipolar ICP generation, although larger pH excursions limit their application to pH insensitive samples.⁷⁵

Scheme 7 illustrates the most commonly used device configurations for focusing analytes by ICP⁹⁶ and fICP.^{34,35,97} Single- and dual-channel preconcentration (Scheme 7a,b) and dual gate (Scheme 7c) designs, are the most common for preconcentration. The dual gate design has a more uniform electric field distribution across the width of the main channel, than do the single and dual-channel preconcentrators, because the voltage is applied on both sides, and ions are depleted symmetrically.^{98,99} The dual gate further allows the driving electrodes to be located in the two electrolyte-filled auxiliary channels that are fluidically isolated from the sample, thereby protecting it from large pH excursions.

Ko et al. developed a U-shaped (**Scheme 7d,f**) device which uses only two driving electrodes. ¹⁰⁰ This U-shaped design has been used for biomolecule preconcentration, however the

electric field is not uniform across all parallel channels. Stronger ICP is observed in channels contacting the portion of the membrane nearest to the ground lead (**Scheme 7f**).

The techniques supported by the designs shown in **Scheme 7g,h,j** are important because they overcome the limitation that ICPF and fICP are traditionally performed as batch processes that have low volume throughput. Split or branching microfluidic devices provide an additional outlet for continuous extraction of focused charged species, micelle-encapsulated uncharged species, particles, and cells (**Scheme 7g**). The fractionation of the sample can be controlled via the ratio of volumetric flow rates in each outlet. This ratio determines the maximum EF, resulting in much more modest enrichment than does accumulation of the analyte (stacking) over a longer period of time. However, it provides access to a sufficient volume of enriched analyte for downstream or off-chip analysis, while transport of an enriched plug results in considerable diffusive broadening. When this branching scheme is utilized in conjunction with fICP, the ability of BPEs to be reconfigured allows for an enriched plug to be directed along the channel while enrichment is maintained³⁶ or transported on-demand to any outlet(s).¹⁰¹ This active control of focused analytes into separate branches is one of the key advantages of fICP.

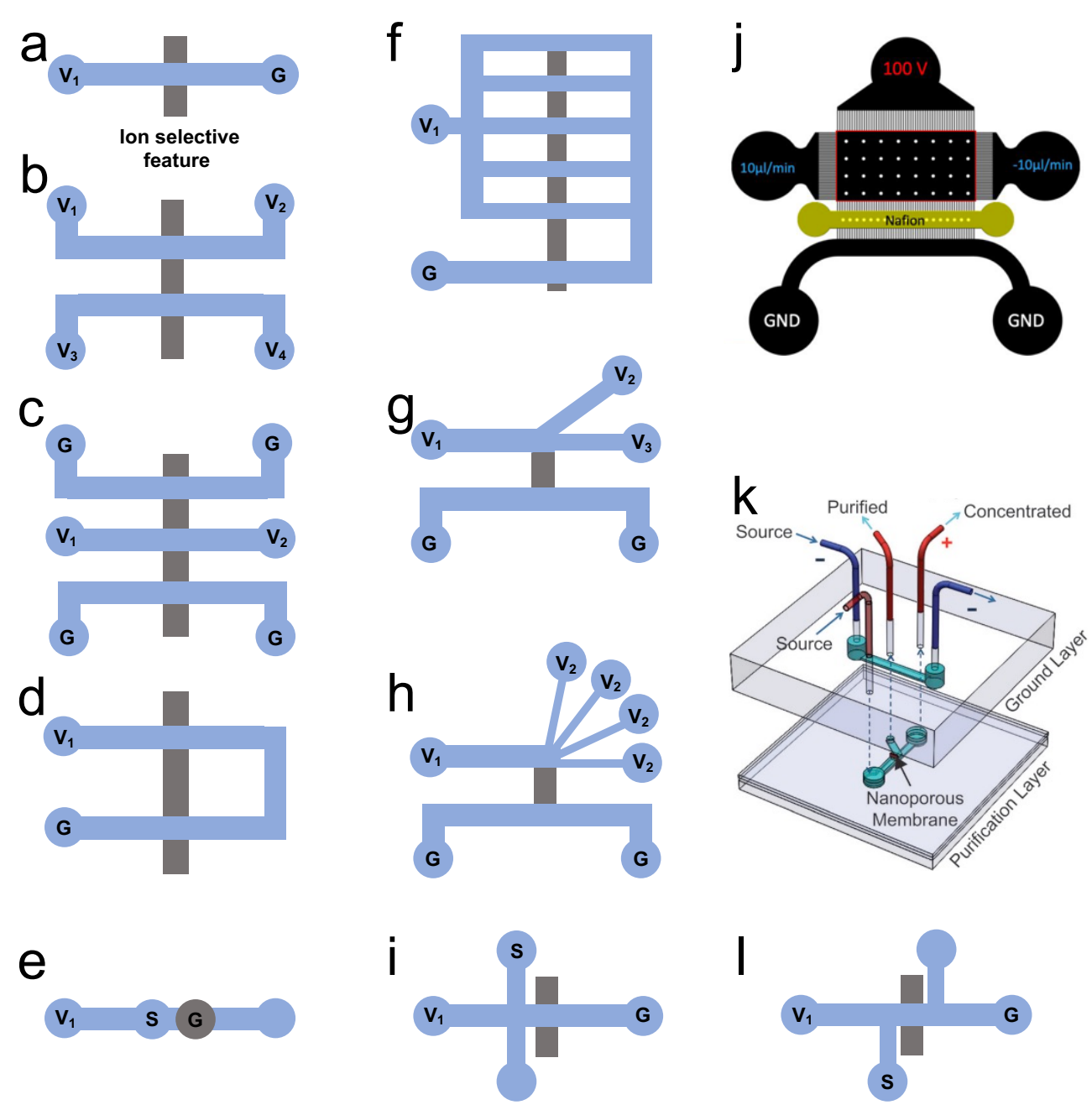
Continuous separation of multiple species is achieved by incorporating multiple channels that are branching at the nanojunction creating a "fan" design (**Scheme 7h**). 102,103 The particles and analytes are deflected from the IDZ to a degree that depends on their electrophoretic mobilities and are thereby directed to distinct outlets. A recent example with important environmental impact is the integration of a multi-outlet device with fICP for sorting of microplastics. 104

Papadimitriou et al. recently developed a method called free flow ICP (FFICP) that yields high resolution separations in a continuously flowing stream. Their device is conceptually similar to the "fan" design in that it has many outlets (**Scheme 7j**). The key distinction is that the

sample solution interacts with the IDZ boundary for a greater duration, which allows for more complete focusing. This outcome is accomplished by employing a combination of pressure driven flow components that, relative the applied electric field, are parallel (for focusing) and perpendicular (to carry the analyte(s) to the outlet).

Scheme 7e,i,l show three variations of a design feature that decouples the sample inlet (indicated as S) from that employed for voltage application and introduction of BGE. 106–108 The sample is introduced in a direction that is orthogonal to focusing. This strategy has two primary advantages. First, a highly conductive sample, such as a biofluid, does not have as great an impact on the electrical resistance of the main (focusing) channel, and therefore, higher spatially-averaged electric field strengths are permitted. The problem of high sample conductivity is conventionally addressed by dilution, which slows mass transport of the analyte to the enriched plug and effectively decreases volumetric throughput. Second, the design prevents biofouling by avoiding contact between the driving electrodes and sensitive samples such as biological cells, bioparticles (such as exosomes) 107 and biomolecules 106,108. A similar outcome can be achieved in a paper-based device by pipetting the sample onto the paper strip during focusing. 88

The out-of-plane device shown in scheme **Scheme 7k** recapitulates the branched layout of **Scheme 7g** but is rotated 90° and extruded to allow a greater contact area between the nanoporous membrane and the sample. This design required the use of a CO₂ laser to create a slot for insertion of a *Nafion* membrane. The auxiliary (grounded channel) lies above the main channel, which is used, in this case, for water desalting.²⁵



Scheme 7. Schematics of various nanofluidic preconcentration device designs including a) single-channel, b) dual-channel, c) dual gate, d) U-shaped, f) U-shaped with parallel concentrators, g) branched, h) 'fan-shaped', j) FFICP, and k) out-of-plane. e, i, l) Sample inlet (S) distinct from BGE inlet (V_1) and oriented orthogonal to the channel in which focusing occurs. Illustrations in (h) and (i) reproduced from ref. [105] and [25], respectively, with permission.

3.2. Ion selective features and their fabrication

Several classes of materials can govern selective ion transport, such as nanoporous membranes and hydrogels, bead beds, nanochannels, and nanotubes. These materials are summarized here, taking into consideration the features relevant to their performance, such as critical dimensions, surface charge density, and exposed area.^{53,103}

3.2.1. Ion permselective membranes and hydrogels

Ionic conductivity, hydrophobicity and ease of fabrication are important features to consider when selecting a material for an ion permselective junction. Ion selective resin solutions like *Nafion* (cation selective), and *Sustainion* (anion selective) are commercially available in solution form and therefore are convenient materials for creating nanojunctions. *Nafion* is a sulfonated tetrafluoroethylene-based fluoropolymer with high surface charge of 200-600 mC/m² and has been well characterized owing to its wide application as a proton conductor for proton exchange membrane (PEM) fuel cells. Further, it is highly hydrophobic and resists swelling in water. Therefore, it is an attractive ion selective material. Several methods have been developed to pattern *Nafion*, several of which are briefly summarized in the following paragraph.

The pattern and dimensions of such a resin solution can be defined by microflow patterning, which utilizes a PDMS microfluidic channel that is reversibly bonded to a glass slide. 109 The resin solution is first flushed through the microchannel and then cured to create the membrane (e.g., *Nafion* is cured at 95°C for 10 min). The microchannel used for patterning is then peeled away, and finally, the glass slide with the patterned membrane is plasma treated and irreversibly bonded to the microchannel to be used for ICP. Importantly, surface area and height of the membrane are governed by the volume and composition of the resin solution and the dimensions

of the microchannel dimensions used for patterning. For example, to achieve an approximately 200 nm membrane thickness, Lee et al. filled a 120-μm deep and 200 μm-wide channel with 1.0 μL of the resin solution (5% *Nafion*) and then removed it with suction, leaving only a thin film behind prior to curing. Although membrane dimensions can be controlled well by microflow patterning, this method is restricted to low viscosity resin solutions. Additionally, irreversible bonding of the glass substrate to the PDMS chip can be challenging if the patterned membrane is thicker than 0.5 μm. As the membrane thickness increases, the seal between the glass and PDMS weakens, thus resulting in device failure.

Microcontact printing utilizes a PDMS microstamp to create a surface-patterned ion selective membrane on a glass slide. During this process, the PDMS microstamp is "inked" with the resin solution, which is transferred to the glass slide by applying pressure and is then cured. This patterning method offers less control of the final membrane dimensions, and the membrane dimensions vary due to applied pressure differences while microstamping. The resulting membrane thickness ranges from 0.5 to 1.0 μm, which makes bonding to PDMS challenging.

A mechanical incision method can be utilized to fabricate a high aspect ratio ion selective nanojunction inside a PDMS microchannel.^{24,111} In this process, the junction is created by making a mechanical incision across the main and auxiliary channels with a scalpel. The incision is then bent open, filled with ion selective resin (e.g., 20% *Nafion*), sealed, and cured. Residual resin on the PDMS surface is then removed by repeatedly applying low residue tape. Next, the PDMS with embedded nanojunction is irreversibly bonded to a glass slide following plasma treatment.

A fourth approach is to fabricate microdevices with narrow openings between the main channel and a resin- or hydrogel-filled channel.^{73,112} In this method, the chip is designed with three

parallel microfluidic channels (main, resin, and auxiliary). Resin solution or hydrogel is then injected into the delivery channel and cured. Due to the surface tension at the narrow openings, the resin solution does not fill the neighboring channels. This technique is limited to high viscosity resin solutions (above 12.5% *Nafion* resin solution). The openings must remain small (10-20 μm), and thus fabrication of such microfluidic devices can be somewhat challenging.

3.2.2. Bead beds

As an alternative to ion selective membranes, Syed et al. employed self-assembly of colloidal silica beads (300-900 nm diameter) to create a nanofluidic junction. Self-assembly by evaporation of aqueous phase (1.0 mM phosphate buffer with 0.05 % Tween-20) allowed for creation of a close-packed structure with controlled pore diameter (~45 nm, 15% that of the particle diameter). Additionally, they demonstrated that the surface properties (zeta potential, and therefore ion selectivity) of such colloidal particles can be modified using polyelectrolyte layer-by-layer self-assembly outside the microfluidic chip to achieve high surface charge. Although strong ion depletion occurred and a high EF was achieved (up to 1700-fold), the concentrated plug propagated upstream too rapidly.

3.2.3. Nanotubes

Single-walled carbon nanotubes (SWNTs) provide an alternative nanoporous material for driving ICP.¹¹³ The nanoporous architecture of stacked, entangled SWNTs and the presence of negatively charged carboxy ligands on their surfaces govern ion permselection. It has been

demonstrated that a 60 nm-thick SWNT structure exhibits similar conductance to a 500 nm-thick *Nafion* membrane. The reported SWNT junction was fabricated using a vacuum filtration and film transfer method with the following steps. First, SWNTs were oxidized by suspending them in a strong acid solution (concentrated H₂SO₄:HNO₃ in a 1:3 volume ratio). Second, this SWNT suspension was diluted with ddi water, and the nanotubes were collected on a membrane filter via vacuum filtration. Third, the SWNT and underlying filter were cut to match the junction dimensions and then placed on a clean glass slide. Lastly, the filter was etched with acetone, and the patterned SWNTs were rinsed with isopropyl alcohol. Although the SWNT patterning process is time consuming and labor intensive, the high conductivity, tunable geometry and chemical properties of the SWNTs can enable the development of high throughput and high aspect ratio ICP devices.

3.2.4. Electrodes for fICP

An electrode can be metallic (e.g., Au, Ag, Pt), carbonaceous (e.g., glassy carbon or graphite), semiconducting (e.g., doped Si, boron doped diamond, indium tin oxide) or nonpolarizable (e.g., Ag/AgCl). Several of these materials have been used to create microband electrodes and BPEs in microfluidic devices using standard photolithographic techniques,⁴⁹ such as masking and etching an evaporated metal film or lift-off lithography. Pyrolyzed photoresist carbon (PPC) can be used as an alternative to evaporated metal films.^{97,114}

When deciding on the type of electrodes to drive formation of an IDZ, one must consider the composition of the BGE and what electrochemical reactions are available to modulate local ion concentration. Importantly, species that can be neutralized by oxidation or reduction should be present in the sample solution at sufficiently high concentration such that their neutralization significantly decreases ionic strength. For example, Knust and coworkers described depletion driven by water electrolysis.³⁵ At a cathode, OH⁻ was generated in sufficient quantities to neutralize a significant fraction of the buffer counter ion TrisH⁺. Because the cathode is at a negative potential relative to the driving electrode(s), the resulting electric field gradient can be used for anion focusing. Conversely, at an anode, H⁺ neutralization of CH₃COO⁻ forms an electric field gradient that is appropriate in sign for focusing cations. These reactions were carried out on Au electrodes. However, many electrode materials can drive water electrolysis and differ primarily by the overpotential required to achieve a sufficient rate of H⁺/OH⁻ production. If a high field strength is desired, then the best material has a high overpotential for water electrolysis and is resistant to degradation of the electrode itself. The internal resistance of the material should be low to prevent joule heating. Any chemical reaction that reduces local BGE concentration can be employed for fICP, thus considering available redox reactions in the sample when choosing electrode materials for fICP is important.

Nafion-coated electrodes have been previously used for sensing. 115–117 Kwak et al. employed a Nafion-coated electrode to drive half-cell ICP. 75 In this process, the electrode consumes or produces protons by water electrolysis, while the Nafion coating prevents hydroxide ion transport. Because of this cation selective transport through the Nafion, the faradaic reactions are unipolar. If a Nafion-coated cathode is employed, H⁺ is consumed at the cathode, resulting in IDZ formation. In contrast, if a Nafion-coated anode is used, then H⁺ is generated by water splitting, and an IEZ forms. In practice, these electrodes lead to larger shifts in pH than a Nafion membrane alone because protons are the only charge carriers (instead of other common BGE cations such as Na⁺ or K⁺).

To complete the electrical circuit, there must be current at the driving electrodes. The most commonly used driving electrodes are coiled Pt wire, which readily provide current owing to a low overpotential for water electrolysis and a high surface area, or Ag/AgCl electrodes, in which current is supplied without altering the solution pH. While less expensive materials, such as graphite, may be attractive for point-of-care devices, the added overpotential required to drive faradaic processes at their surface necessitates a higher applied voltage, which may not be practical in a low resource setting. Yoon and coworkers reported a TiO₂ photoanode driving electrode, which provides a route to utilize renewable energy. There are opportunities to develop driving electrodes that provide long-lasting current without altering solution pH, for example, by capacitance or pseudocapacitance.

3.3. Sample composition

3.3.1. Concentration of the analyte and the electrolyte determine the limit of enrichment

Sample composition has a profound influence on the enrichment and separation of charged analytes. As was discussed in previous subsections of this *Tutorial Review*, the concentration of the BGE will influence the EDL thickness and *Du*, which determine the degree of CP. Further, *Du* and co-ion mobility collectively define propagating and non-propagating regimes. The concentration and mobilities of the ions of the BGE and of the analyte(s) are also correlated to the limit of enrichment.

Several studies have shown that a higher EF is achieved for samples with lower initial analyte concentration.^{34,37,55} Numerical simulations showed that this limiting behavior is

attributable to accumulation of the charged analyte to a sufficiently high concentration to impact the shape of the electric field gradient – i.e., the analyte becomes a significant charge carrier. However, Hong et al. demonstrated that under a distinct set of experimental conditions, the EF is independent of the initial concentration of the analyte. ¹²⁰ Ouyang et al. explained this phenomenon by introducing two limiting regimes governed by electrokinetics or by electroneutrality. 121 In the electrokinetically limited regime, the distribution of the ions of the BGE defines the electric field profile, and then enrichment is determined by the balance between convective, electrophoretic and diffusive fluxes of the analyte. This regime is defined by a buffer concentration that is several orders of magnitude greater than that of the analyte. In this regime, the EF depends exponentially on both the Péclet number and the mobility of the analyte relative to its co-ion. This dependency means that enrichment is favored by a high mobility analyte, a slow co-ion, and less diffusive broadening. Conversely, when the analyte is a significant charge carrier, the EF will be limited by the availability of counter-ions to pair with the analyte ions to maintain electroneutrality. EF is therefore directly proportional to the counter-ion concentration and is diminished if the analyte and co-ion are highly mobile, which places a greater demand on the counter-ion. After this limit is reached, arrival of additional analyte will lead to widening of the enriched plug while it remains at a fixed concentration.

3.3.2. Complex matrices in biological and environmental applications

Samples relevant to environmental analysis and human health (e.g., blood plasma) can present additional challenges that complicate analyte focusing by ICP. Due to these challenges, only a handful of applications using complex samples have been reported.^{29,111} For example, direct

contact to the electrodes or membrane can denature proteins and lead to biofouling of these surfaces. Biofouling can be reduced by initiating IDZ formation prior to injection of a complex sample to repel biomolecules from the junction or by changing the position¹¹¹ or material of driving electrodes. For applications in complex matrices, electrode materials that are designed to resist biofouling, such as the nanoporous electrodes developed by Collinson and coworkers, ^{122,123} are promising. Further ion selective membranes with tunable porosity, ion selectivity, and hydrophilicity have been reported, ^{124,125} some of which boast high ion conductivity while being comprised of materials more biocompatible than *Nafion*.

Highly abundant proteins, such as albumin in blood, accumulate during ICP-based enrichment and rapidly reach the concentration limit dictated by electroneutrality. In such case, the enriched plug of protein gradually widens, pushing higher mobility species such as nucleic acids back towards the inlet. Han and coworkers addressed this challenge by applying a pulse of pressure at the sample inlet, resulting in the enriched plug of protein being pushed over the IDZ. This approach allowed the protein to be depleted while the enriched band of nucleic acid was retained.¹²⁶

An additional challenge with working in biofluids is their high native ion concentration (~150 mM), which leads to a thin EDL and therefore, to a weak ICP. In such cases, to achieve EDL overlap and strong CP formation, ion selective features with small nanopores (e.g., *Nafion*, 4 nm) must be used. Finally, there are few faradaic reactions available to drive CP in biofluids, such as neutralization of endogenous weak acids and bases, thus limiting implementation of fICP in more complex matrices. Furthermore, neutralization of anionic species such as bicarbonate at an anode will generate an IDZ that is useful for focusing of only cationic analytes.

The high ionic conductivity of biological fluids results in high currents under an applied field, and the result is rapid water electrolysis at the driving electrodes leading to gas bubble formation and Joule heating that can damage a sample or an ion selective membrane, lead to local changes in viscosity, and uneven thermal conditions within the microfluidic channels. High currents in biological fluids can be reduced by dilution with low conductivity electrolytes^{88,127} or by introduction of the sample orthogonal to the direction of focusing (as in **Scheme 7e,i,l**). 106–108

3.3.3. Additives to the sample for sharper IDZ boundary formation

The viscosity of the media or BGE can influence the IDZ stability and propagation. It has been shown that additives that increase the viscosity of the sample can help achieve higher EF by inhibiting Taylor dispersion. To this end, Gao et al. added 0.10% w/v hydroxyethyl cellulose (HEC, *Natrosol*) to the BGE during cation and anion enrichment in a paper microfluidic device. HEC is a nonionic water-soluble polymer commonly used as a thickening agent in cosmetics and pharmaceutical formulations. Addition of HEC to the BGE decreased the enriched dye band width by ~2.5 fold, while increasing the fluorescence intensity of the enriched band by a factor of 3. It is important to note that additives can also change the axial location of the enriched band due to an inverse relationship between viscosity and electrophoretic mobility. Moreover, the authors noticed an approximately 50% decrease in EF (near to that obtained in the absence of HEC) when a HEC concentration above 0.10% w/v was used. The authors did not comment on the cause of the observed decrease, which may be due to excessive dampening of EOF in the paper strip. Thus, the additive concentration for each system must be optimized.

3.3.4. Additives to alter analyte mobility and to achieve focusing of uncharged species

It has been shown previously that uncharged molecules are not affected by the electric field and are therefore unable to be enriched by ICP.^{20,128} However, a recent study found that an uncharged dye was repelled from the IDZ during ICP in blood plasma, whereas in phosphate buffer solution, redirection of the dye was not observed. This observation was attributed to intermolecular interactions between the uncharged dye and charged species native to blood plasma. ¹²⁹ To further investigate this phenomenon and to address the limitation of ICP to only charged analytes, Berzina et al. recently developed continuous micellar electrokinetic focusing (CMEKF), in which uncharged compounds are focused by ICP *via* their incorporation into an ionic micellar phase. ¹²⁸ This approach combines concepts of micellar electrokinetic chromatography (MEKC) or micellar capillary electrophoresis (micellar CE) with ICPF. ¹³⁰ This new technique has enabled a route to further expand the utility of ICP to applications in which focusing of uncharged species is needed, such as water purification, and pharmaceutical and environmental analysis. This approach is generalizable – any binding event that "assigns" charge, can facilitate ICP-based focusing of uncharged species.

3.4. Analyte encapsulation following ICPF

A significant challenge to the broad application of ICPF for quantitative analysis is that there have been very few demonstrations of *in situ* analysis of the focused analyte(s). Further, their transport to a downstream location or off-chip for analysis leads to unwanted dilution due to dispersion. In response to this challenge, several strategies have been developed to "lock in" and

collect the enriched analyte band(s) for downstream or off-chip analysis. Here, we summarize recent advancements in the encapsulation of a preconcentrated plug using droplet- and valve-based microfluidic platforms.

Sample preconcentration takes place under continuous flow and therefore, suffers from broadening due to Taylor dispersion when the applied electric field is removed. To remove the need for continuous application of an electric field to sustain the concentrated plug, microfluidic droplet generators can encapsulate the analyte into water-in-oil droplets or gel plugs. Encapsulation offers a straightforward way to preserve the sample concentration for further analysis, such as enzyme activity assays and protein immunoassays.

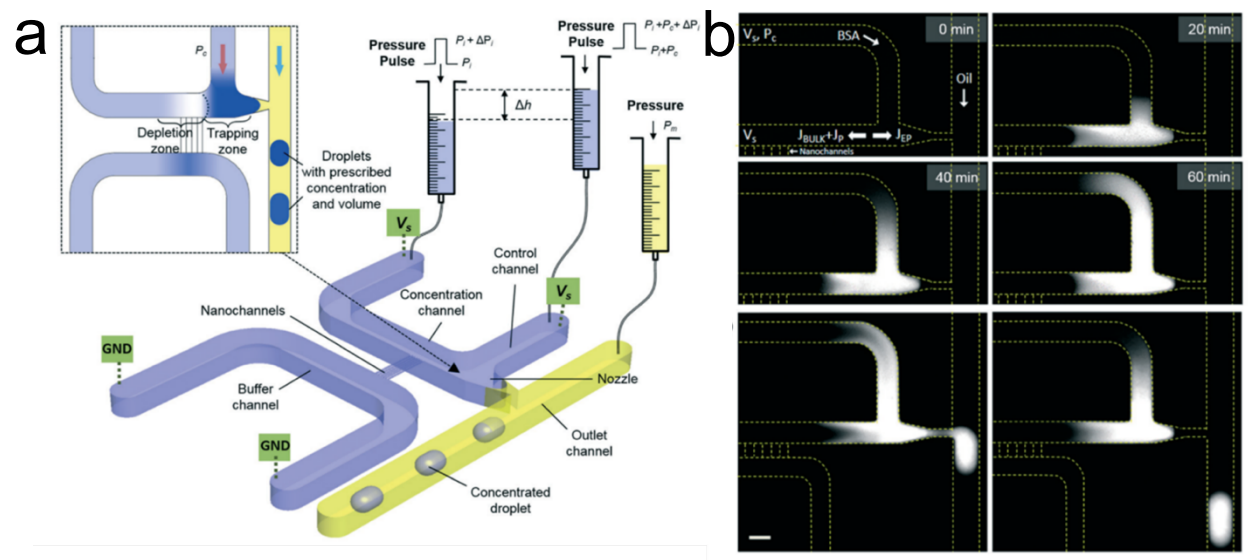


Figure 5. a) Schematic diagram of the nanofluidic concentrator coupled with a droplet-on-demand system; b) Sequential fluorescence images showing the preconcentration process of FITC-BSA in the nanofluidic concentrator at $V_s = 120 \text{ V}$ and $P_c = 1.52 \text{ kPa}$ for 60 min. Here, V_s is the voltage bias applied between the sample and the auxiliary channel across the junction, and P_c is the incremental pressure applied to the control channel relative to that at the sample inlet (P_i) . Illustration reproduced from ref. [132] with permission.

Chen et al. integrated electrokinetic preconcentration with droplet generation to quantify metalloproteinase activity in cell lysate.¹³¹ After the sample was enriched and encapsulated in

droplets, there was a 10-fold better discrimination between stimulated and untreated cell samples, while the required sample size was reduced 100-fold relative to a conventional assay. However, while the plug containing the assay mixture was enriched 100-fold, following its release, the enrichment reduced due to dispersion during transport to the droplet generator. To address this limitation, Yu et al. developed a 'nano-preconcentrator' with a pressure-assisted strategy for positioning the concentrated sample plug directly at the nozzle, which greatly eliminated the concentration decline during sample ejection (**Figure 5**). Using this device design, the authors reported encapsulation of analytes enriched 10⁴-fold.

Phan et al. combined a continuous flow concentrator (branched channel, as in **Scheme 7f**) with a droplet generator in a single device for enriched analyte encapsulation. First, the analyte was preconcentrated by ICP while being redirected into a narrow branching channel. Subsequently, at the end of this channel, the concentrated analyte was enclosed in 25 μ m- to 50 μ m- water-in-oil droplets. ¹³³ In this device, under a flow rate of 10.0 μ L h⁻¹ (0.17 μ L min⁻¹), 100-fold enrichment of charged species from 1.0 μ M to 100 μ M was achieved.

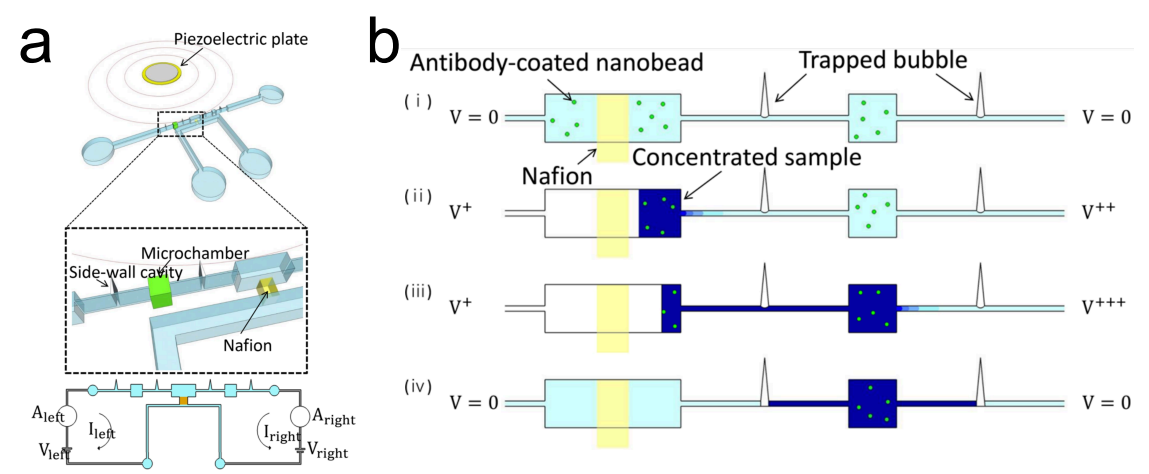


Figure 6. Schematic illustration of a) the electrokinetic preconcentrator with bubble valves, and b) the process by which the concentrated plug of analyte was isolated. Illustration reproduced from ref. [134] with permission.

Although droplets can serve as an excellent tool to encapsulate concentrated analytes, breaking of the microemulsion is required before some types of analysis. Also, hydrophobic analytes can partition into the oil phase, and thus are not good candidates for droplet-based encapsulation using oil. As an alternative, Deng and coworkers developed a bubble valve device to trap preconcentrated analyte plugs using air (**Figure 6**). ¹³⁴ To test the device, low abundance C-reactive protein (CRP) (a biomarker for coronary heart disease and atherosclerosis) was successfully preconcentrated and quantified using bead immunoassay. Up to 10⁴-fold enrichment of target analyte was reported, while improving the limit of detection by 4-fold (to 100 pg mL⁻¹).

Choi et al. developed an ICPF device with integrated pneumatic microvalves located between microchambers.¹⁷ The authors demonstrated control over the location of two enriched and separated analyte bands and prevented dispersion after removing the applied voltage. A separation resolution between dyes of 1.75 with an overall EF of up to 100-fold was achieved.

3.5. In-droplet ICP

Droplet microfluidics has revolutionized biotechnology owing to an ability to encapsulate individual entities (e.g., single nucleic acids, enzymes, or biological cells) for analysis and to segment a time varying sample (e.g., cell secretions or interstitial fluid from tissues) into picoto nanoliter aliquots. In this context, concentration enrichment can potentially lead to an increase in the speed of reactions or assay sensitivity. Moreover, manipulation of droplet composition and ion distribution can create opportunities for mobility-based assays. However, extended periods of analyte accumulation from a bulk sample leads to a loss of single-entity isolation or temporal resolution. To address this challenge, Kim et al. developed a method to manipulate concentration

profiles inside nanoliter-scale water-in-oil droplets by ICP.⁹⁵ This approach achieves both enrichment and separation of charged compounds within a droplet by positioning it between two cation selective membranes that extend along a microchannel like railroad tracks. Each membrane connects the main (droplet) channel to one of two parallel auxiliary channels filled with the BGE (**Figure 7a,b**).

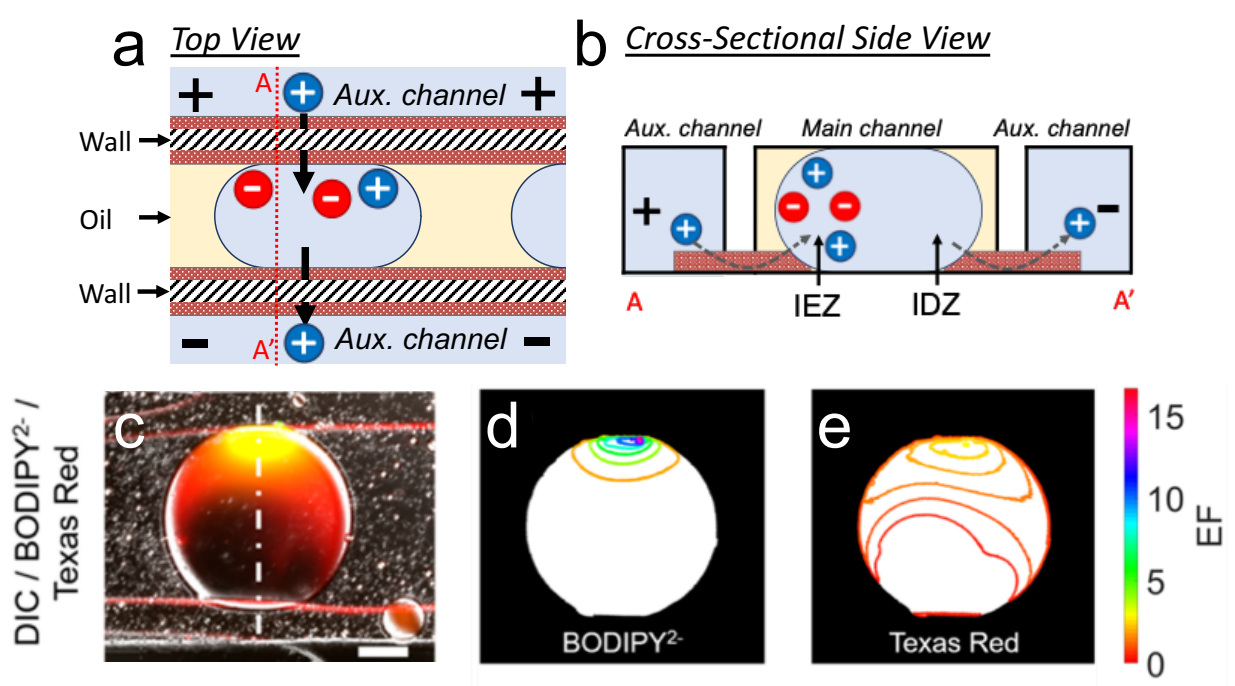


Figure 7. a) Top view and b) cross-sectional side view illustrations of an aqueous droplet positioned between two cation selective membranes (red) in a microfluidic channel. The membranes interconnect the main (droplet) channel with two parallel auxiliary channels filled with the BGE. Under an applied voltage bias as shown, cations are extracted from and injected into the droplet. Anions migrate toward the anodic membrane to maintain electroneutrality and are therefore enriched, generating an IDZ and IEZ within the droplet. c) Overlay of brightfield and green and red fluorescence micrographs of a droplet containing two fluorescent tracers with distinct electrophoretic mobilities. Isometric contour plots show the distribution of the d) green and e) red dyes in the micrographs shown in (c). Illustration modified from ref. [95] with permission.

A voltage bias applied between the auxiliary channels drives ionic current across the cation selective membrane via the droplet. As a result, cations were depleted from the droplet region nearest to the ground auxiliary channel (cathodic channel), while anions migrated towards the

anodic compartment, generating an IDZ and IEZ. 16.7-fold enrichment of an anionic fluorophore (BODIPY disulfonate) and its separation from a second dye (Texas Red) was demonstrated in a 5.5 nL droplet, under 10.0 V voltage bias (**Figure 7c-e**). The in-droplet ICP phenomenon was demonstrated over a wide range of experimental parameters including droplet volume, voltage bias, droplet composition and flow rate. The versatility of this approach indicates a high potential for its application to bioassays, and improvements in speed, sensitivity, and selectivity are expected.

3.6. Multistage and high throughput preconcentration

Existing biomolecule nanoconcentrators can achieve 10^2 - to 10^6 - fold enrichment in one hour, a value limited by the small sample volume (μ L scale) from which the analyte is swept during ICP. To increase the volumetric throughput while also increasing the degree of enrichment, devices with staged parallel and serial enrichment units can be used. A microfluidic device with 4 to 64 parallel enrichment channels arranged radially for high throughput enrichment was designed by Lee et al. (**Figure 8**). Here, a buffer channel-less design simplified device fabrication. In one selection was achieved with printed ion permselective membranes or silver electrodes (for ICP and fICP, respectively) (**Figure 8a,b**). In this device, the diluted sample (35 μ L) was injected at the center using a pipette (**Figure 8**, steps i and ii), and a 10 V DC bias was applied between the radial electrode and a wire electrode inserted in the pipette tip. The preconcentrated plugs of analyte migrated backwards towards the center of the device where they were collected with the pipette tip (**Figure 8**, step iii).

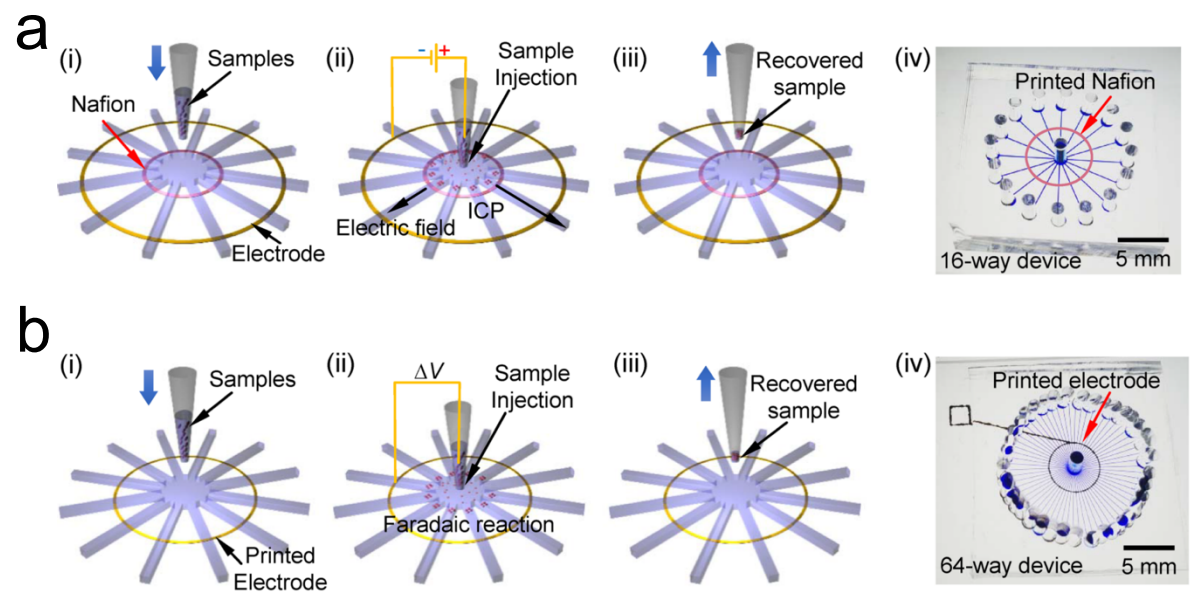


Figure 8. Radial buffer-free preconcentration device with a) *Nafion* junction and b) printed silver electrode. Both devices had the same operating procedure: i) buffer injection and preparation of the sample solution; ii) sample injection and preconcentration of molecules; iii) extraction and recovery of preconcentrated molecules. iv) A photographic image of the devices. Illustration reproduced from ref. [135] with permission.

The nanopreconcentrator yielded moderate recovery ratios for polystyrene particles, fluorescent dye, and dsDNA of 85.5%, 79.0%, and 51.3%, respectively, and the preconcentration factor was poor (up to 10-fold). However, this calculation was based on the concentration of the sample in the collected volume (1 to 5 μ L) and not the maximum concentration achieved within the microfluidic channel. The authors indicated that higher enrichment in a shorter time frame can be achieved using a higher initial sample volume and increasing the number of branching channels.

Recently, Ouyang et al. developed a hierarchical microfluidic molecular enrichment system (HOLMES) that can achieve billion-fold enrichment (10⁹) of biomolecules and proteins within 30 min (**Figure 9a**).⁸³ This high EF is obtained by a four-stage hierarchical concentration process, in which first, parallel nanofluidic concentrators are simultaneously operated to sweep milliliters of sample (up to 10 mL). In this 1st stage, vertically stacked (up to 12) plasma-bonded PDMS layers define chambers, each containing massively parallel microchannels. A

perpendicularly patterned strip of *Nafion* connects these parallel microchannels (blue, **Figure 9b**) to auxiliary channels (green). These concentrators release their contents into successively narrower chambers in the 2nd - 4th stages (**Figure 9c**), in which biomolecule plugs are combined and reconcentrated. The number of parallel microchannels in each chamber is scaled down by 10- or 100-fold per stage.

4. Integration of other analytical methods with ICPF

An important hurdle to the broad application of ICPF is the qualitative and quantitative analysis of the enriched target. Thus far, detection has been largely limited to fluorescent or electroactive species. In this section, we summarize in-line detection methods that have been integrated with ICP and discuss how these techniques are applied to various biological systems.

4.1. Immunoassay

Several microfluidic devices based on ICP have been developed to preconcentrate biomolecules before detection with immunoassays. The increased concentration of the analyte enhances the sensitivity of these assays. Wang et al. were first to integrate a nanopreconcentrator with a bead bed immunoassay. Following 30 min of enrichment of a sample over antibody-modified beads, they achieved more than 500-fold enhanced sensitivity for the fluorescent protein R-phycoerythrin (PE) from 50 pM to the sub-100 fM range. To test the device with a more complex sample, they added 10 µg mL⁻¹ green fluorescent protein (GFP), a non-target protein, to test the influence of an interferent on preconcentration and detection of target molecules. The results

indicated that the interferent was co-enriched, but it was not bound to the beads. Thus, this platform shows promise to preconcentrate and detect charged biomolecules in the presence of interferents.

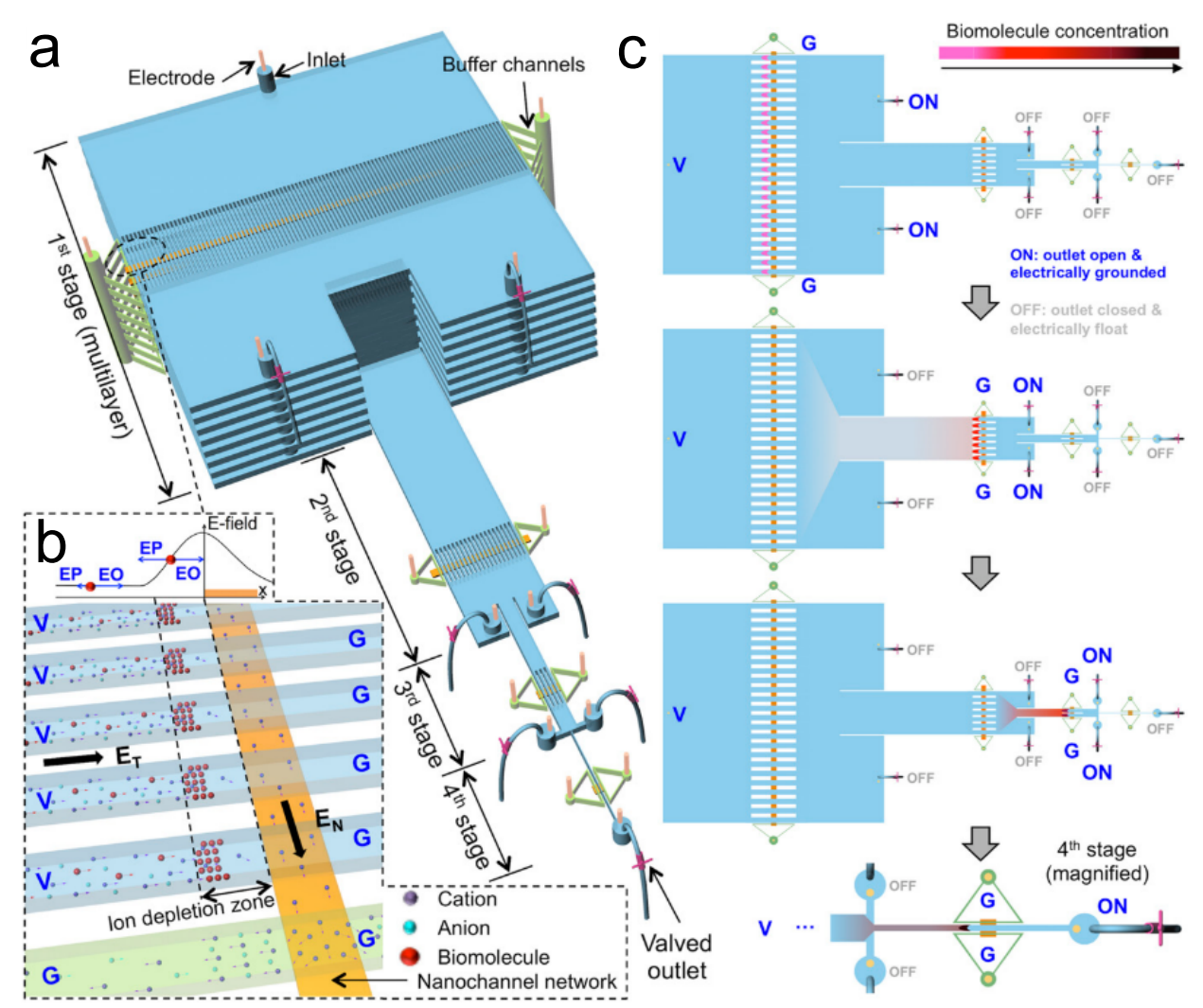


Figure 9. a) Schematic of HOLMES. At each stage, parallel microchannels and buffer channels are bridged by a *Nafion* membrane. b) Schematic of biomolecule enrichment in the parallel channels. Under the electrical configuration shown, biomolecules are electroosmotically injected into the parallel channels and electrokinetically concentrated just upstream of the IDZs induced at the micro-/nano- channel junctions. The membrane interconnects the microchannels (blue) with an auxiliary channel (green). c) Illustration of staged preconcentration of biomolecules including the locations at which driving electrodes apply positive potentials (ON), ground (G), or are left at a floating potential (OFF). Illustration reproduced from ref. [83] with permission.

A similar platform was developed for multiplexed enzyme-linked immunosorbent assay (ELISA). ¹³⁶ In this study, beads modified with antibodies to two prostate cancer-specific antigens were incubated in blood plasma prior to labeling with an enzyme-linked antibody. The beads were then packed into a microchannel, and the substrate for the enzyme flowed across them. ICPF was utilized to enrich the fluorescent product. The sensitivity for the detection of these two cancer markers was enhanced 65- to 100-fold, and five distinct samples were analyzed simultaneously in parallel channels. This same research group later improved multiplexing (up to 128 individually controlled parallel channels) and throughput for this bead-based immunoassay platform. ¹⁰⁰

4.2 Enzymatic assay

There have been several reports in which enzymatic assay rate and sensitivity have been be increased by ICPF. 110,137 Lee et al. demonstrated a decreased assay time from 1 h to 10 min along with a 100-fold enhancement of the sensitivity for trypsin (1.0 pg mL-1). Similarly, ICPF was used to enhance an assay for kinase in cell lysate. The protocol yielded a 25-fold increase in reaction rate and a 65-fold enhancement in sensitivity. These improvements allowed a reduction in sample size from 200 μ L to 5 μ L (equivalent to lysate from \sim 5 cells) and a shortened assay time (from 1 h to 10-25 min). These results show that ICP can potentially enable a route to single-cell analysis.

Recently, Wei et al. developed a multi-well detection platform with integrated electrokinetic pre-concentrators for enzymatic assays.³⁰ They integrated 12 ICP preconcentrators with a standard 12-well plate and demonstrated detection of a metalloproteinase (MMP-9) expression in the breast adenocarcinoma cell line MDA-MB-231. Preconcentration by ICP

allowed a decreased assay time (by 10 h) and an increase in the overall sensitivity of the assay by an order of magnitude. This result is significant because it demonstrates the practical integration of microfluidic preconcentrators with a microplate assay for standard laboratory use.

4.3. Electrochemical sensing

The simultaneous detection of several biomarkers for early diagnosis or prognosis of disease is often challenging due to their extremely low abundance in biological fluids. For example, methylated DNA is believed to be a promising marker for early diagnosis of cancer. However, the concentration level is found to be in the fM range. Electrochemical biosensors have high sensitivity (on the order of 1 nM), enable quantification, and require minimal equipment. Thus, they are good candidates for point-of-care testing. Techniques like ligase chain reaction¹³⁸ and polymerase chain reaction¹³⁹ have been used for methylated DNA amplification, previously. However, they are time consuming and tedious. To address the need for a relatively fast and sensitive detection method, Hong et al. developed a valve-based microfluidic chip, in which methylated DNA was preconcentrated by ICPF and then further quantified using a nanostructured gold biosensor (**Figure 10**).¹²⁰ Using this microfluidic chip, 100- to 120-fold sample preconcentration was obtained in 10 min, which improved the LOD of methylated DNA from 475 pM to 350 fM in buffer.

Nanostructure-based electrical biosensors have been used for ultrasensitive and label-free biomolecule detection. ¹⁴⁰ For example, the electrical resistance of a nanofluidic crystal (NFC) is sensitive to biomolecule binding. However, high sensitivity can only be achieved under low ionic strength conditions, and therefore, sensing under physiological conditions (160 mM) is

challenging. At high ionic strength, surface charges are screened by ions of the BGE, and the EDL has a thickness of < 1 nm.

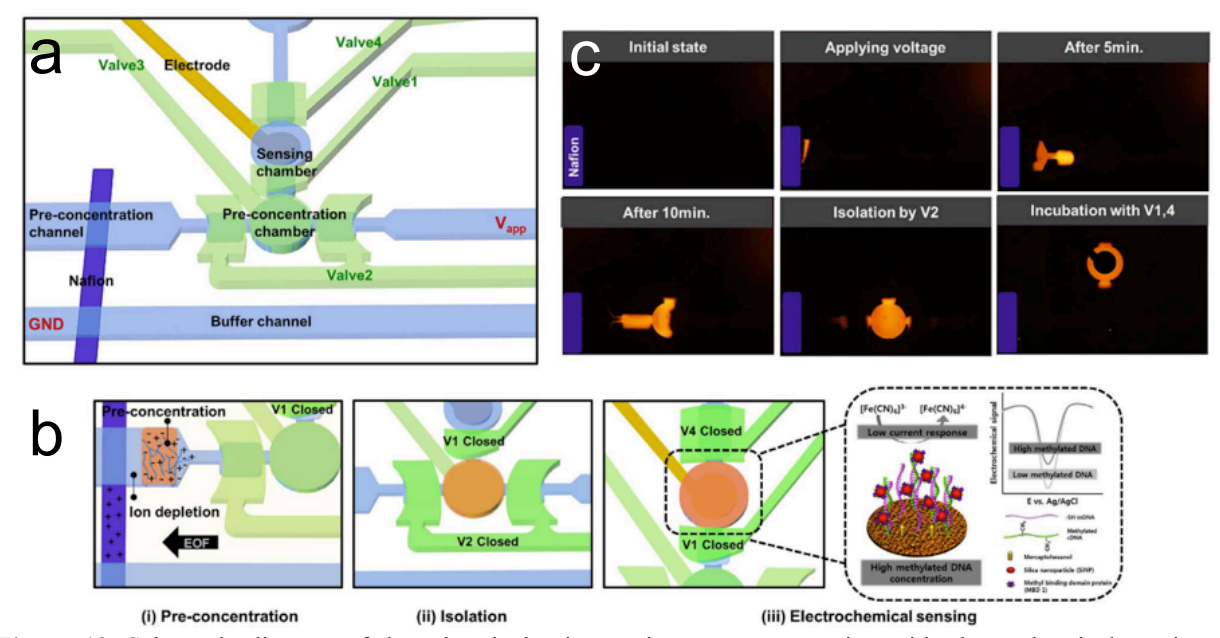


Figure 10. Schematic diagram of the microdevice integrating pre-concentration with electrochemical sensing. a) Schematic diagram of the microfluidic pre-concentration chip; b) working principle of the chip (i) pre-concentration, (ii) isolation and (iii) incubation of the methylated DNA on the electrochemical sensor and in the inset, sensing principle of the electrochemical sensor; c) time-lapse fluorescence images of the DNA pre-concentration and transfer to the sensor. Illustration reproduced from ref. [120] with permission.

Ouyang et al. demonstrated that electrical detection of biomolecules could be achieved by employing ICP to lower the ionic strength at the NFC biosensor following an initial binding step. ¹⁴¹ Their device consisted of two perpendicular channels with nanofilters located on three sides of the intersection to retain functionalized nanoparticles there (**Figure 11**). After loading the sample at the inlet (**Figure 11**, *II*, at location *A*), CP was initiated for biomolecule preconcentration near the NFC (**Figure 11**, *III*). Following the incubation step (**Figure 11**, *III*), CP was initiated again to achieve a local decrease in ion concentration by 200-fold near the NFC to facilitate sensing.

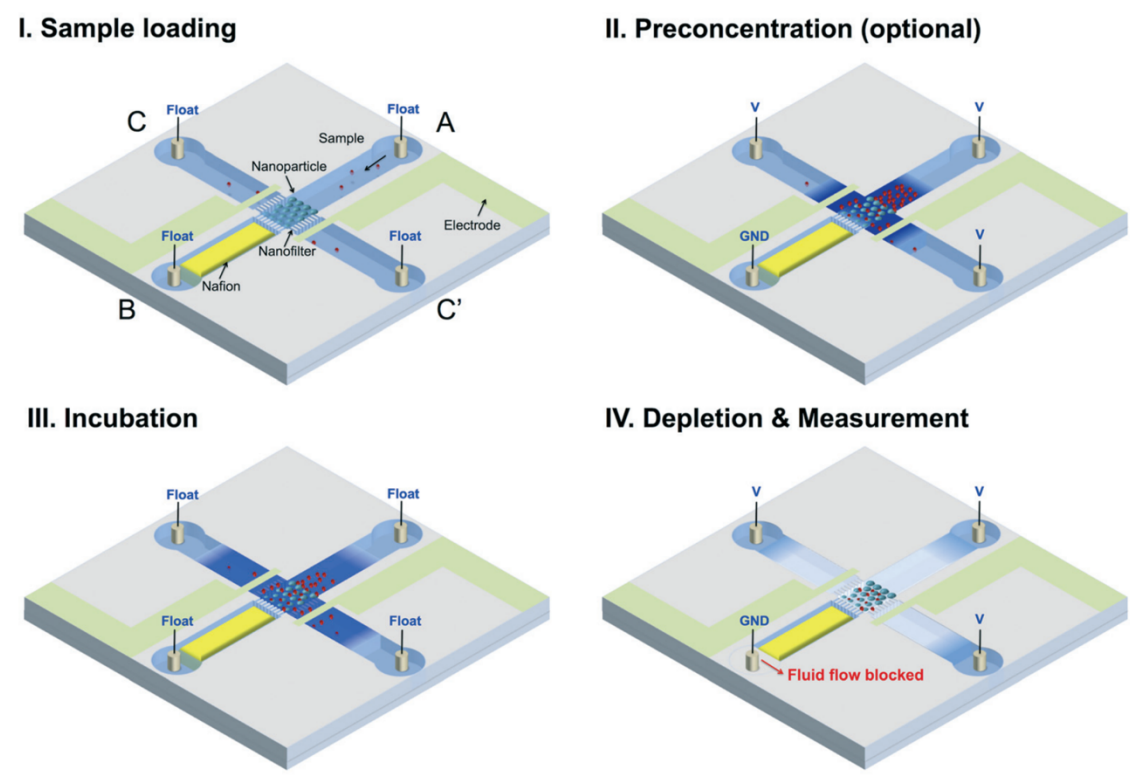


Figure 11. Schematic illustration of the operation of the ICP-coupled nanofluidic crystal for biosensing. Illustration reproduced from ref. [141] with permission.

ICP has been employed not only for analyte preconcentration prior to electrochemical sensing, but also to regenerate sensing substrates. Chen et al. introduced a microfluidic device for real-time continuous bioassays without the requirement of a separate clean buffer solution for rinsing steps (**Figure 12**).²⁹ In this 'buffer-free' device, first, an aptamer sensor was employed for measurement of target biomolecules in human serum. Second, the sensor surface was regenerated to allow repeated assays. To achieve the latter goal, the authors sourced purified water from the human serum by ICP-based repulsion of other plasma components into another microfluidic branch. The results showed that in 10 min after applying the driving voltage, the sensors were completely regenerated.

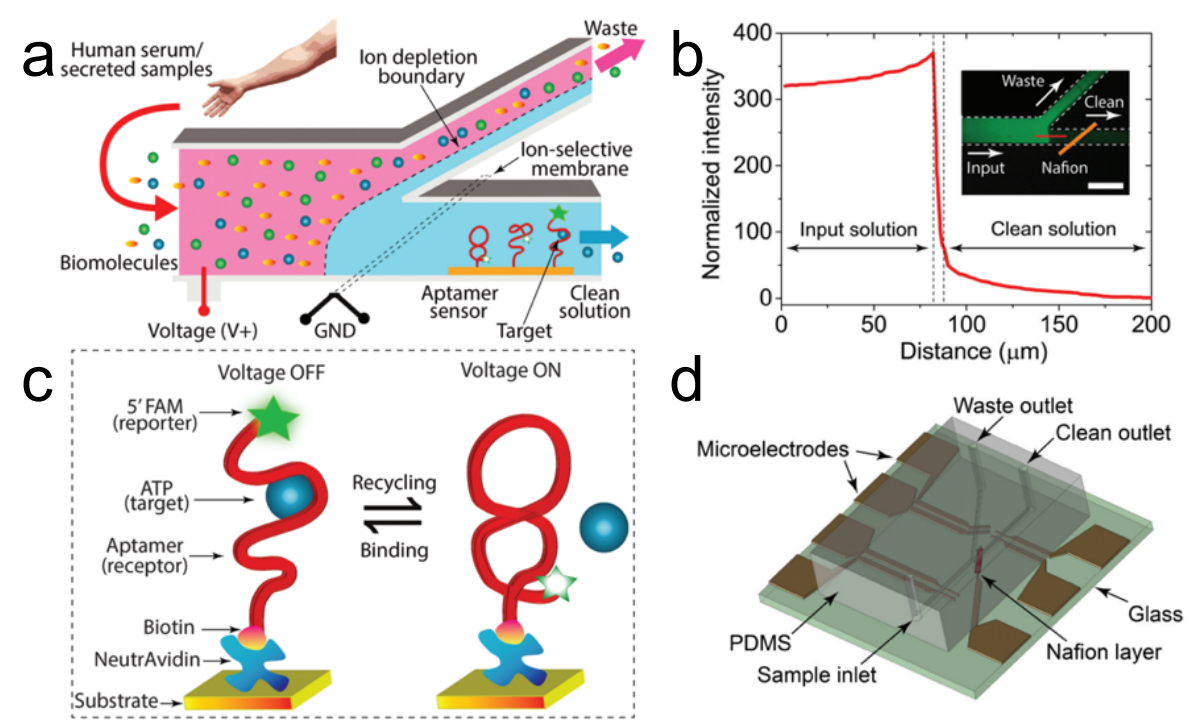


Figure 12. a) Schematic of the nanofluidic device for real-time target biomolecule monitoring; b) the binding of the target biomolecule to the aptamer immobilized on the glass substrate; c) fluorescence micrograph demonstrating ICP-based repulsion of plasma components (green fluorescent dye) into the branching channel (inset scale bar 200 μm); (d) Illustration of the branching microfluidic device with embedded membrane and microelectrodes. Graph demonstrates the normalized fluorescence intensity along the red line across the IDZ. Illustration reproduced from ref. [29] with permission.

4.4. The ICP current-voltage curve as a non-optical sensor

A recent innovation overcomes the need for fluorescently labeled targets by leveraging ICP itself as the sensing mechanism. Ion-selective structures respond to a voltage bias with a distinctive nonlinear current-voltage curve that has ohmic, limiting and overlimiting regions (*Section 2.4.*). Chang and coworkers demonstrated that binding events that confine charged molecules to the surface of an ion permselective membrane significantly alter the shape of its current-voltage curve. 142,143 For example, hybridization of negatively charged DNA to the surface of an anion selective membrane (positively charged) leads to surface charge inversion and changes ion

conductance through the membrane, especially in the overlimiting region. 142,143 These finding suggested that the current-voltage response is sensitive to the presence of charged molecule binding events on the surface of the membrane. Since then, this phenomenon has been used as a reporting mechanism in several assays for biomarkers. 144,145 For example, this method was recently applied to the detection in human serum of ribonucleic acid (RNA) from the mosquito-borne virus that causes dengue fever. 146 The method is label free and requires minimal peripheral equipment, making it well-suited to point-of-care analysis. Four sensors were employed – one specific to each of four serotypes of the dengue virus. Each sensor was an anion selective membrane modified with a probe specific for one serotype. Binding of the target RNA led to a shift in the onset of overlimiting behavior to a higher voltage versus the probe alone. The authors reported excellent specificity, which they attributed to the ability of electroconvection to wash the sensor surface, thereby eliminating non-specific binding. By using this method in concert with upstream one-pot reverse transcriptase PCR (RT-PCR), the authors were able to detect as few as 100 copies of RNA in 1 mL of human plasma.

5. Summary of tips and tricks

Challenge	Tips and Tricks
IDZ instability	 Introduce geometric restrictions (decrease channel height and width). 46 Create an alternate current path through the IDZ by increasing channel surface charge using <i>Nafion</i> coating. 44 Decrease current density at the ion selective structure by increasing its surface area. 72 Add microstructuring to the membrane. 71
IDZ propagation	 Apply pressure driven counterflow. Use dual membranes to define preconcentration in a specific region.⁴⁵ Change ion transport mechanism from ICP to capillarity ICP, in which ion transport is governed by capillary forces and not by an applied external field.⁷³

Uncharged analytes not focused	➤ Neutral species do not migrate in response to an electric field gradient. To achieve neutral species separation, ionic surfactants above their critical micelle concentration can be used. 128
Unwanted pH changes	 Change material of the electrode to avoid oxygen evolution reaction (OER) and hydrogen evolution reaction (HER).⁷⁷ Coat the driving electrode with an ion permselective membrane.⁶⁴ Increase the buffer concentration. Change buffer composition (different pK_a values for various buffers), and ionic strength.⁷⁶
Sample dispersion once electric field is removed	➤ Use droplet-based or valve-based encapsulation. 17,132,134,135
Gas bubble formation and Joule heating	 Sample conductivity may be too high. Dilute the sample to decrease conductivity.^{88,127} Inject the sample orthogonal to the direction of focusing.^{106–108} Apply the voltage between the membrane and an outlet from ion depleted solution exits the device¹¹¹

6. Conclusions and future outlook

In this *Tutorial Review*, we have discussed both fundamental and practical aspects of ICP and fICP and summarized recent advancements relevant to the application of ICPF to quantitative analysis. To use ICP effectively, it is important to understand the mechanisms by which ion permselectivity or faradaic reactions can lead to localized depletion of ions of the BGE, and how the resulting electric field gradients facilitate focusing of analytes in the presence of a counter flow. Many distinct device configurations and methods have been developed for applying the requisite electric and flow fields that drive ICPF, and therefore, we have presented the basic principles and relative advantages of each. The greatest experimental challenges in ICPF are the onset of fluid vortices that lead to unwanted mixing, the upstream propagation of the IDZ boundary and analyte plug, unwanted pH excursions near membranes and electrodes, and at high BGE

conductivities, Joule heating and gas formation. While strategies to address these challenges are ongoing, there are existing approaches to mitigate their effects, which we discussed throughout the *Tutorial Review* and included in subsection 5 – *Summary of tips and tricks*.

For new practitioners, we included a brief summary of device design principles and fabrication methods and a more detailed discussion of materials commonly utilized to facilitate selective ion transport or electrochemical reactions. Given the recent push toward high-throughput preconcentrators and the demand for devices that are easier to fabricate (or to manufacture), there is an opportunity to develop materials and device architectures amenable to larger length scales and mass production. As ICPF devices are adopted into broader use, there is a need for user-friendly computational methods that allow device dimensions and experimental parameters to be optimized for a specific application in silico. ICP poses a significant computational challenge including coupled Poisson, Nernst-Planck, and Navier-Stokes equations, and therefore, approaches that reduce computational load are needed.

We further discussed the impact of the sample composition on ICPF. A key advancement in this area is the introduction of scaling laws that describe the theoretical maximum enrichment factor that can be attained. The scaling laws differentiate two distinct regimes that are defined by the ratio of the concentration of the analyte versus that of the BGE. Enrichment is limited by electrokinetics (peak mode) when this ratio is high and electroneutrality (plateau mode) when it is low. 105,121 We also discussed strategies to address the challenges presented by complex biological matrices, such as high ionic conductivity, non-depleted ions (in fICP), and biofouling, and we summarized additives to improve performance, including viscosity modifiers to increase Péclet number and ionic micelles to alter analyte mobility. This latter advancement has allowed for

separation of neutral species and can be generalized to any intermolecular interaction that would assign charge, thus expanding the applicability of ICPF.

Owing to the low volumetric throughput of most ICPF devices, integration of focusing with on- or off-chip analysis has been limited. We discuss approaches that address this challenge including encapsulation of analytes in water-in-oil droplets to "lock-in" enrichment during transport off-chip and multi-stage (hierarchical) concentrators that dramatically increase both throughput and enrichment rate. Such increased throughput holds promise to provide sufficient volumes and concentration for integration with mass spectrometric analysis or polymerase chain reaction (PCR). In-droplet ICP allows for enrichment and separation in a confined volume, thereby retaining information from time varying samples and isolation of individual entities (e.g., single nucleic acids, enzymes, or biological cells) and can be integrated into existing droplet microfluidic workflows. Finally, we describe progress in the quantification of analytes by interfacing ICP preconcentrators with immunoassays, enzymatic assays, and electrochemical sensing, and we highlight a very recent advancement, in which binding events at an ion-selective membrane are detected via resulting changes in the current-voltage curve obtained during ICP.

In addition to providing background knowledge of ICPF, this Tutorial Review summarizes "tips and tricks" for new practitioners and provides insight into aspects of ICPF most in need of advancement. We anticipate progress in the following areas: rapid or more facile device construction (especially high-throughput) including biocompatible, high surface area, and 3-dimensional materials for the ion-selective junction; methods for addressing high conductivity and biofouling in complex matrices; the development of user-friendly computational models to aid in customization of devices for new applications; methods that leverage intermolecular interactions (such as analyte encapsulation in micelles); integration of high-throughput ICPF with a wider

variety of analytical methods; and extension of recently introduced concepts such as in-droplet ICP and sensing via the ICP current-voltage curve to a wider set of analytical challenges.

CRediT authorship contribution statement

Beatrise Berzina: Writing - original draft. Robbyn Anand: Writing - review & editing.

Declaration of competing interest

The authors declare that they have no known competing financial interests or personal relationships that could have appeared to influence the work reported in this paper.

Acknowledgements

This material is based upon work supported by the National Science Foundation under Grant No. (1849109).

References

- (1) Wong, P. K.; Wang, T. H.; Deval, J. H.; Ho, C. M. Electrokinetics in Micro Devices for Biotechnology Applications. *IEEE/ASME Trans. Mechatronics* **2004**, *9* (2), 366–376. https://doi.org/10.1109/TMECH.2004.828659.
- (2) Burke, J. M.; Smith, C. D.; Ivory, C. F. Development of a Membrane-Less Dynamic Field Gradient Focusing Device for the Separation of Low-Molecular-Weight Molecules. *Electrophoresis* **2010**, *31* (5), 902–909. https://doi.org/10.1002/elps.200900589.
- (3) Sun, X.; Farnsworth, P. B.; Tolley, H. D.; Warnick, K. F.; Woolley, A. T.; Lee, M. L. Performance Optimization in Electric Field Gradient Focusing. *J. Chromatogr. A* **2009**, *1216* (1), 159–164. https://doi.org/10.1016/j.chroma.2008.11.031.
- (4) Lin, S. L.; Li, Y.; Tolley, H. D.; Humble, P. H.; Lee, M. L. Tandem Electric Field Gradient Focusing System for Isolation and Concentration of Target Proteins. *J. Chromatogr. A* **2006**, *1125* (2), 254–262. https://doi.org/10.1016/j.chroma.2006.05.041.
- (5) Humble, P. H.; Kelly, R. T.; Woolley, A. T.; Tolley, H. D.; Lee, M. L. Electric Field Gradient Focusing of Proteins Based on Shaped Ionically Conductive Acrylic Polymer. *Anal. Chem.* **2004**, *76* (19), 5641–5648. https://doi.org/10.1021/ac040055+.
- (6) Koegler, W. S.; Ivory, C. F. Focusing Proteins in an Electric Field Gradient. *J. Chromatogr. A* **1996**, 726 (1–2), 229–236. https://doi.org/10.1016/0021-9673(95)01069-6.
- (7) Sustarich, J. M.; Storey, B. D.; Pennathur, S. Field-Amplified Sample Stacking and Focusing in Nanofluidic Channels. *Phys. Fluids* **2010**, *22* (11). https://doi.org/10.1063/1.3496498.
- (8) Li, C.; Yang, Y.; Craighead, H. G.; Lee, K. H. Isoelectric Focusing in Cyclic Olefin Copolymer Microfluidic Channels Coated by Polyacrylamide Using a UV Photografting

- Method. *Electrophoresis* **2005**, *26* (9), 1800–1806. https://doi.org/10.1002/elps.200410309.
- (9) Jung, B.; Bharadwaj, R.; Santiago, J. G. On-Chip Millionfold Sample Stacking Using Transient Isotachophoresis. *Anal. Chem.* 2006, 78 (7), 2319–2327. https://doi.org/10.1021/ac051659w.
- (10) Malá, Z.; Gebauer, P.; Boček, P. Recent Progress in Analytical Capillary Isotachophoresis. *Electrophoresis* 2015, 36 (1), 2–14. https://doi.org/10.1002/elps.201400337.
- (11) Ross, D.; Locascio, L. E. Microfluidic Temperature Gradient Focusing. *Anal. Chem.* **2002**, 74 (11), 2556–2564. https://doi.org/10.1021/ac025528w.
- (12) Hoebel, S. J.; Balss, K. M.; Jones, B. J.; Malliaris, C. O.; Munson, M. S.; Vreeland, W. N.; Ross, D. Scanning Temperature Gradient Focusing. *Anal. Chem.* 2006, 78 (20), 7186–7190. https://doi.org/10.1021/ac060934r.
- Balss, K. M.; Vreeland, W. N.; Phinney, K. W.; Ross, D. Simultaneous Concentration and Separation of Enantiomers with Chiral Temperature Gradient Focusing. *Anal. Chem.* 2004, 76 (24), 7243–7249. https://doi.org/10.1021/ac049046r.
- (14) Li, M.; Anand, R. K. Recent Advancements in Ion Concentration Polarization. *Analyst* **2016**, *141* (12), 3496–3510. https://doi.org/10.1039/C6AN00194G.
- (15) Leinweber, F. C.; Tallarek, U. Nonequilibrium Electrokinetic Effects in Beds of Ion-Permselective Particles. *Langmuir* 2004, 20 (26), 11637–11648. https://doi.org/10.1021/la048408n.
- (16) Pu, Q.; Yun, J.; Temkin, H.; Liu, S. Ion-Enrichment and Ion-Depletion Effect of Nanochannel Structures. *Nano Lett.* **2004**, *4* (6), 1099–1103. https://doi.org/10.1021/nl0494811.
- (17) Choi, J.; Huh, K.; Moon, D. J.; Lee, H.; Son, S. Y.; Kim, K.; Kim, H. C.; Chae, J. H.; Sung, G. Y.; Kim, H. Y.; et al. Selective Preconcentration and Online Collection of Charged Molecules Using Ion Concentration Polarization. *RSC Adv.* **2015**, *5* (81), 66178–66184. https://doi.org/10.1039/c5ra12639h.

- (18) Cheow, L. F.; Sarkar, A.; Kolitz, S.; Lauffenburger, D.; Han, J. Detecting Kinase Activities from Single Cell Lysate Using Concentration-Enhanced Mobility Shift Assay. *Anal. Chem.* **2014**, *86* (15), 7455–7462. https://doi.org/10.1021/ac502185v.
- (19) Zangle, T. A.; Mani, A.; Santiago, J. G. Theory and Experiments of Concentration Polarization and Ion Focusing at Microchannel and Nanochannel Interfaces. *Chem. Soc. Rev.* **2010**, *39* (3), 1014. https://doi.org/10.1039/b902074h.
- (20) Kim, S. J.; Song, Y. A.; Han, J. Nanofluidic Concentration Devices for Biomolecules Utilizing Ion Concentration Polarization: Theory, Fabrication, and Applications. *Chem. Soc. Rev.* **2010**, *39* (3), 912–922. https://doi.org/10.1039/b822556g.
- Wang, C.; Wang, Y.; Zhou, Y.; Wu, Z. Q.; Xia, X. H. High-Performance Bioanalysis Based on Ion Concentration Polarization of Micro-/Nanofluidic Devices. *Anal. Bioanal. Chem.* **2019**, *411* (18), 4007–4016. https://doi.org/10.1007/s00216-019-01756-8.
- (22) Fu, L. M.; Hou, H. H.; Chiu, P. H.; Yang, R. J. Sample Preconcentration from Dilute Solutions on Micro/Nanofluidic Platforms: A Review. *Electrophoresis* **2018**, *39* (2), 289–310. https://doi.org/10.1002/elps.201700340.
- (23) Hlushkou, D.; Knust, K. N.; Crooks, R. M.; Tallarek, U. Numerical Simulation of Electrochemical Desalination. *J. Phys. Condens. Matter* **2016**, *28* (19), 0–28. https://doi.org/10.1088/0953-8984/28/19/194001.
- (24) Kim, S. J.; Ko, S. H.; Kang, K. H.; Han, J. Direct Seawater Desalination by Ion Concentration Polarization. *Nat. Nanotechnol.* 2010, 5 (4), 297–301. https://doi.org/10.1038/nnano.2010.34.
- (25) MacDonald, B. D.; Gong, M. M.; Zhang, P.; Sinton, D. Out-of-Plane Ion Concentration Polarization for Scalable Water Desalination. *Lab Chip* 2014, 14 (4), 681–685. https://doi.org/10.1039/C3LC51255J.
- (26) Roelofs, S. H.; Van Den Berg, A.; Odijk, M. Microfluidic Desalination Techniques and Their Potential Applications. *Lab Chip* 2015, *15* (17), 3428–3438. https://doi.org/10.1039/c5lc00481k.
- (27) Kwak, R.; Kim, S. J.; Han, J. Continuous-Flow Biomolecule and Cell Concentrator by Ion

- Concentration Polarization. *Anal. Chem.* **2011**, *83* (19), 7348–7355. https://doi.org/10.1021/ac2012619.
- (28) Anand, R. K.; Johnson, E. S.; Chiu, D. T. Negative Dielectrophoretic Capture and Repulsion of Single Cells at a Bipolar Electrode: The Impact of Faradaic Ion Enrichment and Depletion. *J. Am. Chem. Soc.* **2015**, *137* (2), 776–783. https://doi.org/10.1021/ja5102689.
- (29) Phan, D.-T.; Jin, L.; Wustoni, S.; Chen, C.-H. Buffer-Free Integrative Nanofluidic Device for Real-Time Continuous Flow Bioassays by Ion Concentration Polarization. *Lab Chip* **2018**, *18* (4), 3962–3979. https://doi.org/10.1039/C7LC01066D.
- (30) Wei, X.; Do, V. Q.; Pham, S. V.; Martins, D.; Song, Y. A. A Multiwell-Based Detection Platform with Integrated PDMS Concentrators for Rapid Multiplexed Enzymatic Assays. *Sci. Rep.* **2018**, *8* (1), 1–11. https://doi.org/10.1038/s41598-018-29065-7.
- (31) Yu, S.; Jeon, T. J.; Kim, S. M. Active Micromixer Using Electrokinetic Effects in the Micro/Nanochannel Junction. *Chem. Eng. J.* 2012, 197, 289–294. https://doi.org/10.1016/j.cej.2012.05.044.
- (32) Chiu, P. H.; Chang, C. C.; Yang, R. J. Electrokinetic Micromixing of Charged and Non-Charged Samples near Nano-Microchannel Junction. *Microfluid. Nanofluidics* **2013**, *14* (5), 839–844. https://doi.org/10.1007/s10404-012-1116-2.
- (33) Jännig, O.; Nguyen, N. T. A Polymeric High-Throughput Pressure-Driven Micromixer Using a Nanoporous Membrane. *Microfluid. Nanofluidics* **2011**, *10* (3), 513–519. https://doi.org/10.1007/s10404-010-0685-1.
- (34) Anand, R. K.; Sheridan, E.; Knust, K. N.; Crooks, R. M. Bipolar Electrode Focusing: Faradaic Ion Concentration Polarization. *Anal. Chem.* **2011**, *83* (6), 2351–2358. https://doi.org/10.1021/ac103302j.
- (35) Knust, K. N.; Sheridan, E.; Anand, R. K.; Crooks, R. M. Dual-Channel Bipolar Electrode Focusing: Simultaneous Separation and Enrichment of Both Anions and Cations. *Lab Chip* **2012**, *12* (20), 4107. https://doi.org/10.1039/c2lc40660h.
- (36) Perdue, R. K.; Laws, D. R.; Hlushkou, D.; Tallarek, U.; Crooks, R. M. Bipolar Electrode

- Focusing: The Effect of Current and Electric Field on Concentration Enrichment. *Anal. Chem.* **2009**, *81* (24), 10149–10155. https://doi.org/10.1021/ac901913r.
- (37) Hlushkou, D.; Perdue, R. K.; Dhopeshwarkar, R.; Crooks, R. M.; Tallarek, U. Electric Field Gradient Focusing in Microchannels with Embedded Bipolar Electrode. *Lab Chip* **2009**, *9* (13), 1903–1913. https://doi.org/10.1039/b822404h.
- (38) Davies, C. D.; Yoon, E.; Crooks, R. M. Continuous Redirection and Separation of Microbeads by Faradaic Ion Concentration Polarization. *ChemElectroChem* **2018**, *5* (6), 877–884. https://doi.org/10.1002/celc.201700450.
- (39) Kim, S. J.; Wang, Y.-C.; Lee, J. H.; Jang, H.; Han, J. Concentration Polarization and Nonlinear Electrokinetic Flow near Nanofluidic Channel. *Phys. Rev. Lett.* 2007, 99 (4), 1–9. https://doi.org/10.1109/TMI.2012.2196707.
- (40) Zhou, K.; Kovarik, M. L.; Jacobson, S. C. Surface-Charge Induced Ion Depletion and Sample Stacking near Single Nanopores in Microfluidic Devices. *J. Am. Chem. Soc.* 2008, 130 (27), 8614–8616. https://doi.org/10.1021/ja802692x.
- (41) Mani, A.; Zangle, T. A.; Santiago, J. G. On the Propagation of Concentration Polarization from Microchannel-Nanochannel Interfaces. Part I: Analytical Model and Characteristic Analysis. *Langmuir* **2009**, *25* (6), 3898–3908. https://doi.org/10.1021/la803317p.
- (42) Zangle, T. A.; Mani, A.; Santiago, J. G. On the Propagation of Concentration Polarization from Microchannel-Nanochannel Interfaces Part II: Numerical and Experimental Study Thomas. *Langmuir* 2009, 25 (12), 3909–3916. https://doi.org/10.1021/la803318e.
- (43) Kim, S. M.; Burns, M. A.; Hasselbrink, E. F. Electrokinetic Protein Preconcentration Using a Simple Glass/ Poly(Dimethylsiloxane) Microfluidic Chip. *Anal. Chem.* 2006, 78 (14), 4779–4785. https://doi.org/10.1021/ac060031y.
- (44) Kim, J.; Cho, I.; Lee, H.; Kim, S. J. Ion Concentration Polarization by Bifurcated Current Path. *Sci. Rep.* **2017**, *7* (1), 1–12. https://doi.org/10.1038/s41598-017-04646-0.
- (45) Kwak, R.; Kang, J. Y.; Kim, T. S. Spatiotemporally Defining Biomolecule Preconcentration by Merging Ion Concentration Polarization. *Anal. Chem.* **2016**, *88* (1), 988–996. https://doi.org/10.1021/acs.analchem.5b03855.

- (46) Kim, K.; Kim, W.; Lee, H.; Kim, S. J. Stabilization of Ion Concentration Polarization Layer Using Micro Fin Structure for High-Throughput Applications. *Nanoscale* 2017, 9 (10), 3466–3475. https://doi.org/10.1039/C6NR08978J.
- (47) Nam, S.; Cho, I.; Heo, J.; Lim, G.; Bazant, M. Z.; Moon, D. J.; Sung, G. Y.; Kim, S. J. Experimental Verification of Overlimiting Current by Surface Conduction and Electro-Osmotic Flow in Microchannels. *Phys. Rev. Lett.* **2015**, *114* (11), 1–5. https://doi.org/10.1103/PhysRevLett.114.114501.
- (48) Crooks, R. M. Principles of Bipolar Electrochemistry. *ChemElectroChem* **2016**, *3* (3), 357–359. https://doi.org/10.1002/celc.201500549.
- (49) Fosdick, S. E.; Knust, K. N.; Scida, K.; Crooks, R. M. Bipolar Electrochemistry. *Angew. Chemie Int. Ed.* **2013**, *52* (40), 10438–10456. https://doi.org/10.1002/anie.201300947.
- (50) Davies, C. D.; Yoon, E.; Crooks, R. M. Continuous Redirection and Separation of Microbeads by Faradaic Ion Concentration Polarization. *ChemElectroChem* 2017, 4, 1–9. https://doi.org/10.1002/celc.201700450.
- (51) Sheridan, E.; Hlushkou, D.; Knust, K. N.; Tallarek, U.; Crooks, R. M. Enrichment of Cations via Bipolar Electrode Focusing. *Anal. Chem.* **2012**, *84* (17), 7393–7399. https://doi.org/10.1021/ac301101b.
- (52) Hlushkou, D.; Dhopeshwarkar, R.; Crooks, R. M.; Tallarek, U. The Influence of Membrane Ion-Permselectivity on Electrokinetic Concentration Enrichment in Membrane-Based Preconcentration Units. *Lab Chip* 2008, 8 (7), 1153–1162. https://doi.org/10.1039/b800549d.
- (53) Kim, M.; Jia, M.; Kim, T. Ion Concentration Polarization in a Single and Open Microchannel Induced by a Surface-Patterned Perm-Selective Film. *Analyst* **2013**, *138* (5), 1370. https://doi.org/10.1039/c2an36346a.
- (54) Jia, M.; Kim, T. Multiphysics Simulation of Ion Concentration Polarization Induced by a Surface-Patterned Nanoporous Membrane in Single Channel Devices. *Anal. Chem.* **2014**, *86* (20), 10365–10372. https://doi.org/10.1021/ac502726u.
- (55) Wang, Y. C.; Stevens, A. L.; Han, J. Million-Fold Preconcentration of Proteins and

- Peptides by Nanofluidic Filter. *Anal. Chem.* **2005**, 77 (14), 4293–4299. https://doi.org/10.1021/ac050321z.
- (56) Cheow, L. F.; Han, J. Continuous Signal Enhancement for Sensitive Aptamer Affinity Probe Electrophoresis Assay Using Electrokinetic Concentration. *Anal. Chem.* 2011, 83 (18), 7086–7093. https://doi.org/10.1021/ac201307d.
- (57) Choi, J.; Baek, S.; Kim, H. C.; Chae, J. H.; Koh, Y.; Seo, S. W.; Lee, H.; Kim, S. J. Nanoelectrokinetic Selective Preconcentration Based on Ion Concentration Polarization. *Biochip J.* **2020**, *14* (1), 100–109. https://doi.org/10.1007/s13206-020-4109-3.
- (58) Baek, S.; Choi, J.; Son, S. Y.; Kim, J.; Hong, S.; Kim, H. C.; Chae, J. H.; Lee, H.; Kim, S. J. Dynamics of Driftless Preconcentration Using Ion Concentration Polarization Leveraged by Convection and Diffusion. *Lab Chip* 2019, 19 (19), 3190–3199. https://doi.org/10.1039/c9lc00508k.
- (59) Lee, H.; Choi, J.; Jeong, E.; Baek, S.; Kim, H. C.; Chae, J. H.; Koh, Y.; Seo, S. W.; Kim, J. S.; Kim, S. J. DCas9-Mediated Nanoelectrokinetic Direct Detection of Target Gene for Liquid Biopsy. *Nano Lett.* 2018, *18* (12), 7642–7650. https://doi.org/10.1021/acs.nanolett.8b03224.
- (60) Tallarek, U.; Perdue, R. K.; Crooks, R. M.; Hlushkou, D.; Laws, D. R. Bipolar Electrode Focusing: Simultaneous Concentration Enrichment and Separation in a Microfluidic Channel Containing a Bipolar Electrode. *Anal. Chem.* 2009, 81 (21), 8923–8929. https://doi.org/10.1021/ac901545y.
- (61) Duffy, D. C.; McDonald, J. C.; Schueller, O. J. A.; Whitesides, G. M. Rapid Prototyping of Microfluidic Systems in Poly(Dimethylsiloxane). *Anal. Chem.* 1998, 70 (23), 4974– 4984. https://doi.org/10.1021/ac980656z.
- (62) Hellmich, W.; Regtmeier, J.; Duong, T. T.; Ros, R.; Anselmetti, D.; Ros, A. Poly(Oxyethylene) Based Surface Coatings for Poly(Dimethylsiloxane) Microchannels. *Langmuir* 2005, 21 (16), 7551–7557. https://doi.org/10.1021/la0510432.
- (63) Doherty, E. A. S.; Meagher, R. J.; Albarghouthi, M. N.; Barron, A. E. Microchannel Wall Coatings for Protein Separations by Capillary and Chip Electrophoresis. *Electrophoresis*

- **2003**, 24 (12), 34–54. https://doi.org/10.1002/elps.200390029.
- (64) Kim, S. J.; Li, L. D.; Han, J. Amplified Electrokinetic Response Concentration Polarization near Nanofluidic Channel. *Langmuir* 2009, 25 (13), 7759–7765. https://doi.org/10.1021/la900332v.
- (65) Yossifon, G.; Chang, H. C. Changing Nanoslot Ion Flux with a Dynamic Nanocolloid Ion-Selective Filter: Secondary Overlimiting Currents Due to Nanocolloid-Nanoslot Interaction. *Phys. Rev. E Stat. Nonlinear, Soft Matter Phys.* **2010**, *81* (6), 1–6. https://doi.org/https://journals.aps.org/pre/abstract/10.1103/PhysRevE.81.066317.
- (66) Zaltzman, B.; Rubinstein, I. Electro-Osmotic Slip and Electroconvective Instability. *J. Fluid Mech.* **2007**, *579* (October), 173–226. https://doi.org/10.1017/S0022112007004880.
- (67) Rubinstein, I.; Shtilman, L. Voltage against Current Curves of Cation Exchange Membranes. J. Chem. Soc. Faraday Trans. 2 Mol. Chem. Phys. 1979, 75 (6), 231–246. https://doi.org/10.1039/F29797500231.
- (68) Rubinshtein, I.; Zaltzman, B.; Pretz, J.; Linder, C. Experimental Verification of the Electroosmotic Mechanism of Overlimiting Conductance through a Cation Exchange Electrodialysis Membrane. *Russ. J. Electrochem.* **2002**, *38* (8), 853–863. https://doi.org/10.1023/A:1016861711744.
- (69) Park, S. Y.; Russo, C. J.; Branton, D.; Stone, H. A. Eddies in a Bottleneck: An Arbitrary Debye Length Theory for Capillary Electroosmosis. *J. Colloid Interface Sci.* 2006, 297
 (2), 832–839. https://doi.org/10.1016/j.jcis.2005.11.045.
- (70) Dydek, E. V.; Zaltzman, B.; Rubinstein, I.; Deng, D. S.; Mani, A.; Bazant, M. Z. Overlimiting Current in a Microchannel. *Phys. Rev. Lett.* **2011**, *107* (11), 1–5. https://doi.org/10.1103/PhysRevLett.107.118301.
- (71) De Valença, J.; Jõgi, M.; Wagterveld, R. M.; Karatay, E.; Wood, J. A.; Lammertink, R. G.
 H. Confined Electroconvective Vortices at Structured Ion Exchange Membranes.
 Langmuir 2018, 34 (7), 2455–2463. https://doi.org/10.1021/acs.langmuir.7b04135.
- (72) Yossifon, G.; Mushenheim, P.; Chang, Y. C.; Chang, H. C. Eliminating the Limiting-Current Phenomenon by Geometric Field Focusing into Nanopores and Nanoslots. *Phys.*

- *Rev. E Stat. Nonlinear, Soft Matter Phys.* **2010**, *81* (4), 1–13. https://doi.org/10.1103/PhysRevE.81.046301.
- (73) Oh, Y.; Lee, H.; Son, S. Y.; Kim, S. J.; Kim, P. Capillarity Ion Concentration Polarization for Spontaneous Biomolecular Preconcentration Mechanism. *Biomicrofluidics* **2016**, *10* (1), 1–12. https://doi.org/10.1063/1.4939434.
- (74) Mai, J.; Miller, H.; Hatch, A. V. Spatiotemporal Mapping of Concentration Polarization Induced PH Changes at Nanoconstrictions. ACS Nano 2012, 6 (11), 10206–10215. https://doi.org/10.1021/nn304005p.
- (75) Kwak, R.; Han, J. Half-Cell Ion Concentration Polarization on Nafion-Coated Electrode. *J. Phys. Chem. Lett.* **2018**, *9* (11), 2991–2999. https://doi.org/10.1021/acs.jpclett.8b01214.
- (76) Andersen, M. B.; Rogers, D. M.; Mai, J.; Schudel, B.; Hatch, A. V.; Rempe, S. B.; Mani, A. Spatiotemporal PH Dynamics in Concentration Polarization near Ion-Selective Membranes. *Langmuir* 2014, 30 (26), 7902–7912. https://doi.org/10.1021/la5014297.
- (77) Kim, W.; Oh, J.; Kwon, S.; Kim, K.; Kim, S. J. Quantifying the PH Shift Induced by Selective Anodic Electrochemical Reactions in the Ion Concentration Polarization Phenomenon. *Lab Chip* **2019**, *19* (8), 1359–1369. https://doi.org/10.1039/c8lc01363b.
- (78) Cheng, L. J.; Chang, H. C. Microscale PH Regulation by Splitting Water. *Biomicrofluidics* **2011**, *5* (4). https://doi.org/10.1063/1.3657928.
- (79) Cheng, L. J.; Chang, H. C. Switchable PH Actuators and 3D Integrated Salt Bridges as New Strategies for Reconfigurable Microfluidic Free-Flow Electrophoretic Separation. *Lab Chip* **2014**, *14* (5), 979–987. https://doi.org/10.1039/c3lc51023a.
- (80) Ren, K.; Zhou, J.; Wu, H. Materials for Microfluidic Chip Fabrication. *Acc. Chem. Res.* 2013, 46 (11), 2396–2406. https://doi.org/10.1021/ar300314s.
- (81) Camino, C.; Lomakin, S. M.; Lazzari, M. Polydimethylsiloxane Thermal Degradation Part
 1. Kinetic Aspects. *Polymer (Guildf)*. 2001, 42 (6), 2395–2402.
 https://doi.org/10.1016/S0032-3861(00)00652-2.
- (82) McDonald, J. C.; Whitesides, G. M. Poly (Dimethylsiloxane) as a Material for

- Fabricating Microfluidic Devices. *Acc. Chem. Res.* **2002**, *35* (7), 491–499. https://doi.org/10.1021/ac001132d.
- (83) Ouyang, W.; Han, J. Universal Amplification-Free Molecular Diagnostics by Billion-Fold Hierarchical Nanofluidic Concentration. *Proc. Natl. Acad. Sci.* **2019**, *116* (33), 16240–16249. https://doi.org/10.1073/pnas.1904513116.
- (84) Hong, S. A.; Kim, Y.-J.; Kim, S. J.; Yang, S. Electrochemical Detection of Methylated DNA on a Microfluidic Chip with Nanoelectrokinetic Pre-Concentration. *Biosens*. *Bioelectron.* 2018, 107, 103–110. https://doi.org/10.1016/J.BIOS.2018.01.067.
- (85) Pi, H.; Tong, J.; Bian, C.; Xia, S. 3D Printed Micro/Nanofluidic Preconcentrator for Charged Sample Based on Ion Concentration Polarization. *J. Micromechanics Microengineering* 2017, 27 (5). https://doi.org/10.1088/1361-6439/aa6151.
- (86) O'Neill, P. F.; Azouz, A. Ben; M. Vázquez, J. L.; Marczak, S.; Slouka, Z.; Chang, H. C.; Diamond, D.; Brabazon, D. Advances in Three-Dimensional Rapid Prototyping of Microfluidic Devices for Biological Applications. *Biomicrofluidics* 2014, 8 (5). https://doi.org/10.1063/1.4898632.
- (87) Waheed, S.; Cabot, J. M.; Macdonald, N. P.; Lewis, T.; Guijt, R. M.; Paull, B.; Breadmore, M. C. 3D Printed Microfluidic Devices: Enablers and Barriers. *Lab Chip* **2016**, *16* (11), 1993–2013. https://doi.org/10.1039/c6lc00284f.
- (88) Gao, H.; Liu, J. J.; Liu, Y. Q.; Wu, Z. Y. Detection of Urine Protein by a Paper-Based Analytical Device Enhanced with Ion Concentration Polarization Effect. *Microfluid*. *Nanofluidics* **2019**, *23* (4), 1–7. https://doi.org/10.1007/s10404-019-2220-3.
- (89) Gao, H.; Xie, M. R.; Liu, J. J.; Fang, F.; Wu, Z. Y. Electrokinetic Stacking on Paper-Based Analytical Device by Ion Concentration Polarization with Ion Exchange Membrane Interface. *Microfluid. Nanofluidics* 2018, 22 (5), 1–8. https://doi.org/10.1007/s10404-018-2071-3.
- (90) Li, X.; Luo, L.; Crooks, R. M. Faradaic Ion Concentration Polarization on a Paper Fluidic Platform. *Anal. Chem.* 2017, 89 (7), 4294–4300. https://doi.org/10.1021/acs.analchem.7b00365.

- (91) Yang, Y.; Noviana, E.; Nguyen, M. P.; Geiss, B. J.; Dandy, D. S.; Henry, C. S. Paper-Based Microfluidic Devices: Emerging Themes and Applications. *Anal. Chem.* 2017, 89 (1), 71–91. https://doi.org/10.1021/acs.analchem.6b04581.
- (92) Son, S. Y.; Lee, H.; Kim, S. J. Paper-Based Ion Concentration Polarization Device for Selective Preconcentration of Muc1 and Lamp-2 Genes. *Micro Nano Syst. Lett.* 2017, 5 (1), 1–5. https://doi.org/10.1186/s40486-017-0042-1.
- (93) Phan, D. T.; Shaegh, S. A. M.; Yang, C.; Nguyen, N. T. Sample Concentration in a Microfluidic Paper-Based Analytical Device Using Ion Concentration Polarization. Sensors Actuators, B Chem. 2016, 222, 735–740. https://doi.org/10.1016/j.snb.2015.08.127.
- (94) Han, S. II; Hwang, K. S.; Kwak, R.; Lee, J. H. Microfluidic Paper-Based Biomolecule Preconcentrator Based on Ion Concentration Polarization. *Lab Chip* **2016**, *16* (12), 2219–2227. https://doi.org/10.1039/c6lc00499g.
- (95) Kim, S.; Ganapathysubramanian, B.; Anand, R. K. Concentration Enrichment, Separation, and Cation Exchange in Nanoliter-Scale Water-in-Oil Droplets. *J. Am. Chem. Soc.* 2020, 142 (6), 3196–3204. https://doi.org/10.1021/jacs.9b13268.
- (96) Son, S. Y.; Lee, S.; Lee, H.; Kim, S. J. Engineered Nanofluidic Preconcentration Devices by Ion Concentration Polarization. *Biochip J.* 2016, 10 (4), 251–261. https://doi.org/10.1007/s13206-016-0401-7.
- (97) Knust, K. N.; Hlushkou, D.; Anand, R. K.; Tallarek, U.; Crooks, R. M. Electrochemically Mediated Seawater Desalination. *Angew. Chemie - Int. Ed.* 2013, 52 (31), 8107–8110. https://doi.org/10.1002/anie.201302577.
- (98) Wang, Y. C.; Han, J. Pre-Binding Dynamic Range and Sensitivity Enhancement for Immuno-Sensors Using Nanofluidic Preconcentrator. *Lab Chip* 2008, 8 (3), 392–394. https://doi.org/10.1039/b717220f.
- (99) Syed, A.; Mangano, L.; Mao, P.; Han, J.; Song, Y.-A. Creating Sub-50 Nm Nanofluidic Junctions in a PDMS Microchip via Self-Assembly Process of Colloidal Silica Beads for Electrokinetic Concentration of Biomolecules. *Lab Chip* **2014**, *14*, 4455–4460.

- https://doi.org/10.1039/c4lc00895b.
- (100) Ko, S. H.; Kim, S. J.; Cheow, L. F.; Li, L. D.; Kang, K. H.; Han, J. Massively Parallel Concentration Device for Multiplexed Immunoassays. *Lab Chip* **2011**, *11* (7), 1351. https://doi.org/10.1039/c0lc00349b.
- (101) Scida, K.; Sheridan, E.; Crooks, R. M. Electrochemically-Gated Delivery of Analyte Bands in Microfluidic Devices Using Bipolar Electrodes. *Lab Chip* **2013**, *13* (12), 2292–2299. https://doi.org/10.1039/c3lc50321f.
- (102) Kim, W.; Park, S.; Kim, K.; Kim, S. J. Experimental Verification of Simultaneous Desalting and Molecular Preconcentration by Ion Concentration Polarization. *Lab Chip* 2017, 17 (22), 3841–3850. https://doi.org/10.1039/C7LC00857K.
- (103) Lee, J. H.; Song, Y. A.; Han, J. Multiplexed Proteomic Sample Preconcentration Device Using Surface-Patterned Ion-Selective Membrane. *Lab Chip* **2008**, *8* (4), 596–601. https://doi.org/10.1039/b717900f.
- (104) Davies, C. D.; Crooks, R. M. Focusing, Sorting, and Separating Microplastics by Serial Faradaic Ion Concentration Polarization. *Chem. Sci.* **2020**. https://doi.org/10.1039/d0sc01931c.
- (105) Papadimitriou, V. A.; Segerink, L. I.; Eijkel, J. C. T. Free Flow Ion Concentration Polarization Focusing (FF-ICPF). *Anal. Chem.* **2020**, *92* (7), 4866–4874. https://doi.org/10.1021/acs.analchem.9b04526.
- (106) Marczak, S.; Senapati, S.; Slouka, Z.; Chang, H. C. Induced Nanoparticle Aggregation for Short Nucleic Acid Quantification by Depletion Isotachophoresis. *Biosens. Bioelectron*. 2016, 86, 840–848. https://doi.org/10.1016/j.bios.2016.07.093.
- (107) Marczak, S.; Richards, K.; Ramshani, Z.; Smith, E.; Senapati, S.; Hill, R.; Go, D. B.; Chang, H. C. Simultaneous Isolation and Preconcentration of Exosomes by Ion Concentration Polarization. *Electrophoresis* 2018, 39 (15), 2029–2038. https://doi.org/10.1002/elps.201700491.
- (108) Zhang, C.; Sun, G.; Senapati, S.; Chang, H. C. A Bifurcated Continuous Field-Flow Fractionation (BCFFF) Chip for High-Yield and High-Throughput Nucleic Acid

- Extraction and Purification. *Lab Chip* **2019**, *19* (22), 3853–3861. https://doi.org/10.1039/c9lc00818g.
- (109) Kim, E.; Xia, Y.; Whitesides, G. M. Polymer Microstructures Formed by Moulding in Capillaries. *Nature* **1995**, *376* (August), 581–584.
- (110) Lee, J. H.; Song, Y. A.; Tannenbaum, S. R.; Han, J. Increase of Reaction Rate and Sensitivity of Low-Abundance Enzyme Assay Using Micro/Nanofluidic Preconcentration Chip. *Anal. Chem.* **2008**, *80* (9), 3198–3204. https://doi.org/10.1021/ac800362e.
- (111) Berzina, B.; Anand, R. K. An Electrokinetic Separation Route to Source Dialysate from Excess Fluid in Blood. *Anal. Chem.* **2018**, *90* (6), 3720–3726. https://doi.org/10.1021/acs.analchem.7b02584.
- (112) Liu, V.; Song, Y.-A.; Han, J. Capillary-Valve-Based Fabrication of Ion-Selective Membrane Junction for Electrokinetic Sample Preconcentration in PDMS Chip. *Lab Chip* 2010, 10, 1485–1490. https://doi.org/10.1039/b923214a.
- (113) Kim, B.; Heo, J.; Kwon, H. J.; Kim, I.; An, T.; Lim, G. Fabrication of Entangled Single-Wall Carbon Nanotube Films as Nanoporous Junctions for Ion Concentration Polarization. *Jpn. J. Appl. Phys.* **2015**, *54* (3), 035102. https://doi.org/10.7567/JJAP.54.035102.
- (114) Ioana Dumitrescu, a D. F. Y. and R. M. C. Characterizing Dual-Electrode Microfluidic Cell for Electrocatalysts. *Lab Chip* 2012, *12*, 986–993. https://doi.org/10.1039/C5EE01452B.
- (115) Szentirmay, M. N.; Martin, C. R. Ion-Exchange Selectivity of Nafion Films on Electrode Surfaces. *Anal. Chem.* **1984**, *56* (11), 1898–1902. https://doi.org/10.1021/ac00275a031.
- (116) Selvaraju, T.; Ramaraj, R. Electrochemically Deposited Nanostructured Platinum on Nafion Coated Electrode for Sensor Applications. *J. Electroanal. Chem.* **2005**, *585* (2), 290–300. https://doi.org/10.1016/j.jelechem.2005.09.005.
- (117) Bobacka, J. Conducting Polymer-Based Solid-State Ion-Selective Electrodes. *Electroanalysis* **2006**, *18* (1), 7–18. https://doi.org/10.1002/elan.200503384.
- (118) Yoon, E.; Davies, C. D.; Hooper, T. A.; Crooks, R. M. Photoelectrochemical Ion

- Concentration Polarization: Membraneless Ion Filtration Based on Light-Driven Electrochemical Reactions. *Lab Chip* **2017**, *17* (14), 2491–2499. https://doi.org/10.1039/c7lc00455a.
- (119) Wang, Y.; Song, Y.; Xia, Y. Electrochemical Capacitors: Mechanism, Materials, Systems, Characterization and Applications. *Chem. Soc. Rev.* 2016, 45 (21), 5925–5950. https://doi.org/10.1039/c5cs00580a.
- (120) Hong, S. A.; Kim, Y. J.; Kim, S. J.; Yang, S. Electrochemical Detection of Methylated DNA on a Microfluidic Chip with Nanoelectrokinetic Pre-Concentration. *Biosens*. *Bioelectron*. **2018**, *107*, 103–110. https://doi.org/10.1016/j.bios.2018.01.067.
- (121) Ouyang, W.; Ye, X.; Li, Z.; Han, J. Deciphering Ion Concentration Polarization-Based Electrokinetic Molecular Concentration at the Micro-Nanofluidic Interface: Theoretical Limits and Scaling Laws. *Nanoscale* **2018**, *10* (32), 15187–15194. https://doi.org/10.1039/c8nr02170h.
- (122) Farghaly, A. A.; Lam, M.; Freeman, C. J.; Uppalapati, B.; Collinson, M. M. Potentiometric Measurements in Biofouling Solutions: Comparison of Nanoporous Gold to Planar Gold. *J. Electrochem. Soc.* 2016, 163 (4), H3083–H3087. https://doi.org/10.1149/2.0101604jes.
- (123) Khan, R. K.; Gadiraju, S. P.; Kumar, M.; Hatmaker, G. A.; Fisher, B. J.; Natarajan, R.; Reiner, J. E.; Collinson, M. M. Redox Potential Measurements in Red Blood Cell Packets Using Nanoporous Gold Electrodes. *ACS Sensors* **2018**, *3* (8), 1601–1608. https://doi.org/10.1021/acssensors.8b00498.
- (124) Bush, A. M.; Ford, H. O.; Gao, F.; Summe, M. J.; Rouvimov, S.; Schaefer, J. L.; Phillip, W. A.; Guo, R. Tunable Mesoporous Films from Copolymers with Degradable Side Chains as Membrane Precursors. *Journal of Membrane Science*. 2018, pp 104–114. https://doi.org/10.1016/j.memsci.2018.08.069.
- (125) Ford, H. O.; Cui, C.; Schaefer, J. L. Comparison of Single-Ion Conducting Polymer Gel Electrolytes for Sodium, Potassium, and Calcium Batteries: Influence of Polymer Chemistry, Cation Identity, Charge Density, and Solvent on Conductivity. *Batteries*

- **2020**, 6 (11), 1–41. https://doi.org/doi:10.3390/batteries6010011.
- (126) Ouyang, W.; Li, Z.; Han, J. Pressure-Modulated Selective Electrokinetic Trapping for Direct Enrichment, Purification, and Detection of Nucleic Acids in Human Serum. *Anal. Chem.* 2018, 90 (19), 11366–11375. https://doi.org/10.1021/acs.analchem.8b02330.
- (127) Han, S. II; Yoo, Y. K.; Lee, J.; Kim, C.; Lee, K.; Lee, T. H.; Kim, H.; Yoon, D. S.; Hwang, K. S.; Kwak, R.; et al. High-Ionic-Strength Pre-Concentration via Ion Concentration Polarization for Blood-Based Biofluids. *Sensors and Actuators, B: Chemical.* 2018, pp 485–493. https://doi.org/10.1016/j.snb.2018.04.144.
- (128) Berzina, B.; Anand, R. K. Continuous Micellar Electrokinetic Focusing of Neutral Species Driven by Ion Concentration Polarization. *Lab Chip* 2019. https://doi.org/10.1039/C9LC00327D.
- (129) Berzina, B.; Anand, R. K. An Electrokinetic Separation Route to Source Dialysate from Excess Fluid in Blood. *Anal. Chem.* **2018**, *90* (6), 3720–3726. https://doi.org/10.1021/acs.analchem.7b02584.
- (130) Muijselaar, P. G.; Otsuka, K.; Terabe, S. Micelles as Pseudo-Stationary Phases in Micellar Electrokinetic Chromatography. *J. Chromatogr. A* **1997**, *780* (1–2), 41–61. https://doi.org/10.1016/S0021-9673(97)00632-8.
- (131) Chen, C. H.; Sarkar, A.; Song, Y. A.; Miller, M. A.; Kim, S. J.; Griffith, L. G.; Lauffenburger, D. A.; Han, J. Enhancing Protease Activity Assay in Droplet-Based Microfluidics Using a Biomolecule Concentrator. *J. Am. Chem. Soc.* **2011**, *133* (27), 10368–10371. https://doi.org/10.1021/ja2036628.
- (132) Yu, M.; Hou, Y.; Zhou, H.; Yao, S. An On-Demand Nanofluidic Concentrator. *Lab Chip* **2015**, *15* (6), 1524–1532. https://doi.org/10.1039/c4lc01480d.
- (133) Phan, D. T.; Chun, Y.; Nguyen, N. T. A Continuous-Flow Droplet-Based Concentrator Using Ion Concentration Polarization. *RSC Adv.* **2015**, *5* (55), 44336–44341. https://doi.org/10.1039/c5ra07491f.
- (134) Deng, C. Z.; Fan, Y. J.; Chung, P. S.; Sheen, H. J. A Novel Thermal Bubble Valve Integrated Nanofluidic Preconcentrator for Highly Sensitive Biomarker Detection. *ACS*

- Sensors 2018, 3 (7), 1409–1415. https://doi.org/10.1021/acssensors.8b00323.
- (135) Lee, S.; Park, S.; Kim, W.; Moon, S.; Kim, H.-Y.; Lee, H.; Kim, S. J. Nanoelectrokinetic Bufferchannel-Less Radial Preconcentrator and Online Extractor by Tunable Ion Depletion Layer. *Biomicrofluidics* **2019**, *13* (3), 034113. https://doi.org/10.1063/1.5092789.
- (136) Cheow, L. F.; Ko, S. H.; Kim, S. J.; Kang, K. H.; Han, J. Increasing the Sensitivity of ELISA Using Multiplexed Electrokinetic Concentrator. *Anal. Chem.* **2010**, *82* (8), 3383–3388. https://doi.org/10.1021/ac9024335.
- (137) Jeong, H. L.; Cosgrove, B. D.; Lauffenburger, D. A.; Han, J. Microfluidic Concentration-Enhanced Cellular Kinase Activity Assay. *J. Am. Chem. Soc.* **2009**, *131* (30), 10340–10341. https://doi.org/10.1021/ja902594f.
- (138) Koo, K. M.; Wee, E. J. H.; Rauf, S.; Shiddiky, M. J. A.; Trau, M. Microdevices for Detecting Locus-Specific DNA Methylation at CpG Resolution. *Biosens. Bioelectron*. 2014, 56, 278–285. https://doi.org/10.1016/j.bios.2014.01.029.
- (139) Md. Hakimul Haque a, b, Vinod Gopalan a, n, Sharda Yadav b, c, Md Nazmul Islam b, c, Ehsan Eftekhari c, d, Qin Li c, d, Laura G. Carrascosa e, Nam-Trung Nguyen c, Alfred K. Lam a, n, M. J. A. S. Detection of Regional DNA Methylation Using DNA-Graphene Affinity Interactions. *Biosens. Bioelectron.* 2017, 87, 615–621. https://doi.org/10.1016/j.bios.2016.09.016.
- (140) Luo, X.; Davis, J. J. Electrical Biosensors and the Label Free Detection of Protein Disease Biomarkers. *Chem. Soc. Rev.* **2013**, *42* (13), 5944–5962. https://doi.org/10.1039/c3cs60077g.
- (141) Ouyang, W.; Han, J.; Wang, W. Enabling Electrical Biomolecular Detection in High Ionic Concentrations and Enhancement of the Detection Limit Thereof by Coupling a Nanofluidic Crystal with Reconfigurable Ion Concentration Polarization. *Lab Chip* 2017, 17 (22), 3772–3784. https://doi.org/10.1039/c7lc00722a.
- (142) Senapati, S.; Slouka, Z.; Shah, S. S.; Behura, S. K.; Shi, Z.; Stack, M. S.; Severson, D. W.; Chang, H. C. An Ion-Exchange Nanomembrane Sensor for Detection of Nucleic Acids

- Using a Surface Charge Inversion Phenomenon. *Biosens. Bioelectron.* **2014**, *60*, 92–100. https://doi.org/10.1016/j.bios.2014.04.008.
- (143) Slouka, Z.; Senapati, S.; Shah, S.; Lawler, R.; Shi, Z.; Stack, M. S.; Chang, H. C. Integrated, DC Voltage-Driven Nucleic Acid Diagnostic Platform for Real Sample Analysis: Detection of Oral Cancer. *Talanta* 2015, 145, 35–42. https://doi.org/10.1016/j.talanta.2015.04.083.
- (144) Taller, D.; Richards, K.; Slouka, Z.; Senapati, S.; Hill, R.; Go, D. B.; Chang, H. C. On-Chip Surface Acoustic Wave Lysis and Ion-Exchange Nanomembrane Detection of Exosomal RNA for Pancreatic Cancer Study and Diagnosis. *Lab Chip* **2015**, *15* (7), 1656–1666. https://doi.org/10.1039/c5lc00036j.
- (145) Ramshani, Z.; Zhang, C.; Richards, K.; Chen, L.; Xu, G.; Stiles, B. L.; Hill, R.; Senapati, S.; Go, D. B.; Chang, H. C. Extracellular Vesicle MicroRNA Quantification from Plasma Using an Integrated Microfluidic Device. *Commun. Biol.* **2019**, *2* (1), 1–9. https://doi.org/10.1038/s42003-019-0435-1.
- (146) Yin, Z.; Ramshani, Z.; Waggoner, J. J.; Pinsky, B. A.; Senapati, S.; Chang, H. C. A Non-Optical Multiplexed PCR Diagnostic Platform for Serotype-Specific Detection of Dengue Virus. Sensors Actuators, B Chem. 2020, 310 (December 2019), 127854. https://doi.org/10.1016/j.snb.2020.127854.